J. Fluid Mech. (1994), *vol.* 280, *pp.* 199–225

The linear stability of boundary-layer flow over compliant walls: effects of boundary-layer growth

By K. S. YEO, B. C. KHOO AND W. K. CHONG

Department of Mechanical and Production Engineering, National University of Singapore, Kent Ridge, Singapore 0511, Republic of Singapore

(Received 11 July 1992 and in revised form 21 June 1994)

The linear stability of boundary-layer flow over compliant or flexible surfaces has been studied by Carpenter & Garrad (1985), Yeo (1988) and others on the assumption of local flow parallelism. This assumption is valid at large Reynolds numbers. Non-parallel effects due to growth of the boundary layer gain in significance and importance as one gets to lower Reynolds number. This is especially so for a compliant surface, which can sustain a variety of wall-related instabilities in addition to the Tollmien–Schlichting instabilities (TSI) that are found over rigid surfaces. The present paper investigates the influence of boundary-layer non-parallelism on the TSI and wall-related travelling-wave flutter (TWF) on compliant layers. Corrections to the growth rate of locally parallel theory for boundary-layer non-parallelism are obtained through a multiple-scale analysis. The results indicate that flow non-parallelism has an overall destabilizing influence on the TSI and TWF. Flow non-parallelism is also found to have a very strong destabilizing effect on the branch of TWF that stretches to low Reynolds number. The results obtained have important implications for the design and use of compliant layers at low Reynolds numbers.

1. Introduction

The stability of boundary-layer flow over compliant or flexible surfaces has evoked considerable interest in recent years. Besides the intrinsic scientific interest, this attention has also been motivated by the potential applications of compliant surfaces as transition-delaying devices and related uses in the area of flow noise control. The idea of using compliant surfaces to stabilize boundary-layer flow has generally been attributed to Kramer (1960).

Thanks to the works of the early pioneers, notably Benjamin (1960, 1963) and Landahl (1962), it is by now well-known that laminar boundary layers over flexible surfaces are susceptible to a wide range of instabilities: Tollmien–Schlichting instabilities (TSI), travelling-wave flutter (TWF), static divergence instability and Kelvin–Helmholtz (KH) instability. The last three instabilities have their origin in wall flexibility and have been termed collectively flow-induced surface instabilities (FISI) by Carpenter & Garrad (1985) and compliance-induced flow instabilities by Yeo (1986, 1988). The linear stability of flow over plate surfaces and viscoelastic layers has been studied in great detail by Carpenter & Garrad (1985, 1986) and Yeo (1986, 1988) respectively. They found that the flow over compliant walls with suitable properties may indeed be stabilized. On the experimental front, Gaster (1987) demonstrated convincingly that flexible viscoelastic layers can indeed reduce the growth of disturbance waves in boundary layers. Moreover, the observed growth of the disturbance waves is in broad agreement with theoretical predictions. Compliant walls

with novel Grosskreutz-type properties (Grosskreutz 1971) have been investigated by Carpenter & Morris (1990) and Yeo (1986, 1990) and found to possess the potential for delaying transition. The stability of three-dimensional linear wave modes over compliant surfaces has also been studied. Yeo (1986, 1992) and Joslin, Morris & Carpenter (1991) found that properly designed compliant walls are able to stabilize three-dimensional linear wave modes and hence achieve significant delay of transition, even though these modes may grow more rapidly than two-dimensional ones. The status of compliant-wall flow stability research was recently reviewed by Carpenter (1990) and Riley, Gad-el-Hak & Metcalfe (1988).

With the linear aspects reasonably well studied, the last few years have witnessed a burgeoning of interest in the nonlinear- and secondary-instability aspects of compliant-wall boundary-layer flow stability; see Joslin & Morris (1992), Thomas (1992) and others. Joslin & Morris found that wall compliance has a suppressing influence on secondary instability of Herbert-type (Herbert 1984). Thomas found that a flexible wall response greatly enriches the possibilities for the occurrence of Craik-type resonant triads (Craik 1971), with some triad combinations displaying exceptionally large interaction coefficients. In the enthusiasm to investigate the interesting problems of the post-linear regimes, a potentially important aspect of compliant-wall boundary-layer instability, namely the boundary-layer non-parallelism, has been largely overlooked, with the exception of a short paper by Carpenter & Sen (1990). The focus of the present paper is on the effects of boundary-layer non-parallelism on compliant-wall flow stability. This non-parallelism arises from the growth of the boundary layer as it develops downstream. There has been fairly extensive investigation into the effects of the non-parallelism on boundary layers over rigid walls. Below, we briefly review the important developments in that area because of their direct relevance to the present study.

The effect of flow divergence or non-parallelism on boundary-layer stability over rigid surfaces was extensively studied in the seventies by Barry & Ross (1970), Bouthier (1972, 1973), Gaster (1974), Saric & Nayfeh (1975), Smith (1979) and others. The objective of these studies was to explain the differences which had emerged between experimentally determined neutral stability results and accurately computed locally parallel-flow results which had become available then; the earlier asymptotic predictions of Shen (1954) were in substantially better agreement with the experimental results. A particularly important non-parallel work of this period is Gaster (1974). Gaster employed a scheme of successive approximation to determine the leading-order $O(\epsilon)$ non-parallel correction to an accurately computed locally parallel solution of the Orr–Sommerfeld (OS) equation, which is applicable strictly to parallel flow. A similar type of $O(\epsilon)$ correction, based on a multiple-scale expansion, was developed by Saric & Nayfeh. Gaster's work is particularly significant in the emphasis he placed on the definition of *disturbance growth*. His results revealed strong dependence of the neutral curves on the criterion of disturbance growth, hence demonstrating that meaningful comparison can only be made between theoretical predictions and experimental results if identical criteria of growth are used. Unfortunately, Gaster's results show a critical Reynolds number of 480 which, while representing an improvement over the locally parallel prediction of 520, is still significantly above the 400 obtained in the experiments of Schubauer & Skramstad (1947) and Ross *et al.* (1970). Saric & Nayfeh's results showed rather better agreement with the experimental results, but it turned out that the criterion of disturbance growth they had used was incompatible with the modes of experimental measurements. This was rectified in a subsequent publication (Saric & Nayfeh 1977). Gaster's results were verified by the independent calculations of Van

Stijn & Van de Vooren (1983) using a different procedure. The multiple-scale approach to obtaining the $O(\epsilon)$ correction for non-parallelism was also used by Bridges & Morris (1987), who propose an alternative neutral-curve criterion.

Two other non-parallel works, generically different in approach from the works cited above and from each other, should also be mentioned. Smith (1979) applied a triple-deck asymptotic scheme to the non-separable partial differential equations of linear flow stability to develop the non-parallel lower neutral branch of TSI. His scheme has been regarded by some as a more rational approach to non-parallel stability calculations because it treats all terms of equal order in the basic flow and the governing equations together, whereas in the correction approach of Gaster and others, some of the higher-order terms are embedded within the OS base solution. However, owing to its sole reliance on asymptotics to develop the solution, Smith's non-parallel results are affected by slow convergence in the parallel-flow part of the series (see his figure 1). The correction approach, on the other hand, is highly expedient in utilizing an available accurate numerically solved parallel-flow solution as a starting point. The Smith scheme is also more complex to apply because the mathematical character of the decks must be selected to match the anticipated solution eigenstructures, which can differ for different instabilities or different parts of the same instability, and additional decks may have to be introduced accordingly. Overall, the correction approach is easier to apply when many different instabilities are to be considered. The effectiveness of the correction approach was recently verified by Fasel & Konzelmann (1990) in a work of a completely different style. Fasel & Konzelmann investigated the problem of boundary-layer non-parallelism through a direct numerical integration of the Navier–Stokes equations. In spite of the distinctly different methodology, their results display remarkable agreement with the neutral curves of Gaster (1974) and Bridges & Morris (1987). Their results therefore affirm the essential soundness of Gaster's scheme and the multiple-scale approach in developing corrections to locally parallel results, and the adequacy of the leading-order correction $O(\epsilon)$ that has hitherto been applied. Fasel & Konzelmann attributed the differences between their results and the experimental results to possible unknown bias in those experiments, which were conducted in the 1940s and the late 1960s.

The effects of boundary-layer non-parallelism on flow stability over plate-type compliant surfaces were recently studied by Carpenter & Sen (1990). Their non-parallel stability calculation, which differs methodologically from those described above, is based on an *extended* form of the OS equation, which is purported to account for all non-parallel effects to $O(\epsilon^1)$. Some neutral stability curves and maximum amplification results pertaining to the growth of TS waves were presented, but the associated physical entity was not clearly defined. They found the effects of non-parallelism on their TSI to be generally small, albeit a little stronger than for rigid-wall TSI. They did not, however, investigate the effects of non-parallelism on the FISI, which comprises among others, the static-divergence, the KH and the TWF instabilities. Boundary-layer non-parallelism holds little significance for the static-divergence and KH instabilities, which are reckoned to be strong absolute instabilities. The TWF, on the other hand, is a convective instability that occurs frequently on compliant walls which exhibit potential for delaying transition. The effects of non-parallelism on TWF modes, and in particular the low-$R_\delta B_2$ branch (see Yeo 1988), is as yet unknown and is of special interest here.

The present paper investigates the two-dimensional non-parallel stability of boundary-layer flow over layered compliant walls. A correction scheme was used because of the availability of accurate locally parallel $O(\epsilon^0)$ solutions (Yeo 1986, 1988)

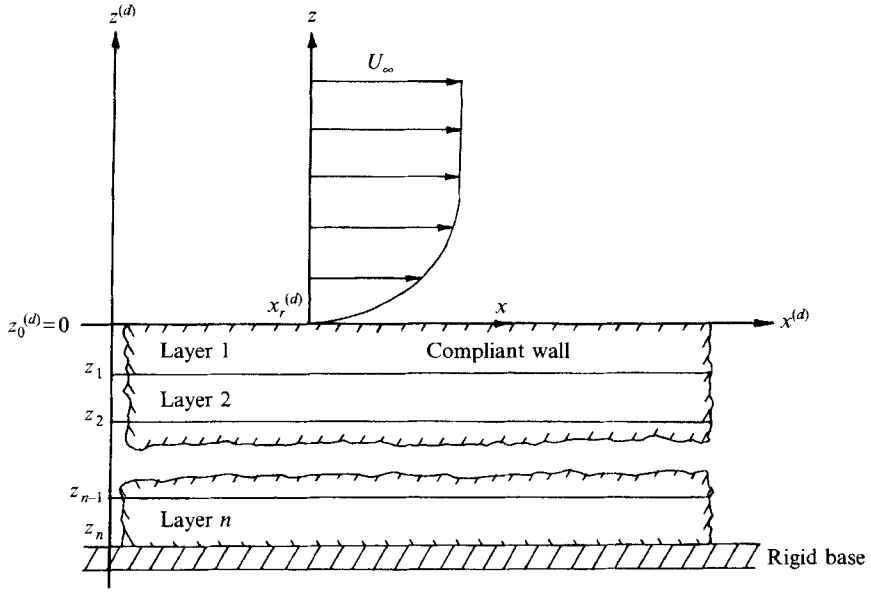

FIGURE 1. Boundary-layer flow over a multi-layer compliant wall: $(x,z)^{(d)}$ is the global reference frame for the stability problem; (x,z) is the local coordinate frame with origin at $(x_r^{(d)},0)$.

which can serve as bases for perturbation. The multiple-scale form was chosen in preference to Gaster's scheme because of its well-established procedure and fairly straightforward application to the present problem. At $O(\epsilon^1)$, the growing equations of the flow, the wall and the boundary conditions are mostly non-homogeneous. The non-homogeneous wall perturbation equations are solved in closed form (involving quadrature). A non-parallel correction of $O(\epsilon^1)$ to the $O(\epsilon^0)$ spatial growth rate of the locally parallel theory is obtained via the solvability condition for the $O(\epsilon^1)$ problem. The solvability condition assumes a fairly complex form because of the presence of non-homogeneous high-order derivative boundary conditions at $O(\epsilon^1)$.

2. Theoretical formulation

Figure 1 shows schematically a two-dimensional boundary-layer flow over a compliant wall which may comprise one or more uniformly thick layers of homogeneous isotropic viscoelastic materials, backed by a rigid base. The *global* coordinate frame, which may also be assumed to be the dimensional coordinate frame, for the stability problem is $(x,z)^{(d)}$, which has its positive x-axis pointing in the streamwise direction. The surface of the compliant wall in the unperturbed state spans the $(x,y)^{(d)}$-plane at $z^{(d)} = z_0^{(d)} = 0$.

The physical system of boundary-layer flow and compliant wall is assumed to be perturbed by a very small disturbance oscillating with a real frequency ω. We are interested in the spatial evolution (development) of such wavy disturbances, taking into account the slow variation of the boundary-layer velocity profile in the streamwise direction. A multiple-scale perturbation scheme is employed to decouple the rapid scale of wavy motion from the slow modulating scale of boundary-layer growth. The multiple-scale analysis is applied below to the equations governing the perturbations in the flow domain, a single-layer compliant wall, and the interface boundary conditions in §§2.1, 2.2 and 2.3 respectively. In §2.4, the locally parallel flow eigenvalue

problem is posed and corrections to the parallel-flow spatial eigenvalue based on various criteria of disturbance growth are developed. Extension of the theory to multi-layer walls is taken up in §2.5.

2.1. *Flow stability equations*

Before proceeding with the formal theoretical development, it is appropriate to state clearly the reference frame and the scaling parameters. The dynamics of wave perturbations in the flow is considered here in a *local* rectangular Cartesian frame (x, z) with its origin at $(x_r, 0)^{(d)}$ in the global frame, see figure 1. The non-dimensionalization reference scales for the local frame (x, z) are: $\delta_r^{(d)}$, the dimensional displacement thickness of the boundary layer at $(x_r, 0)^{(d)}$; $U_\infty^{(d)}$, the dimensional free-stream velocity of the boundary layer; and $\rho_f^{(d)}$, the dimensional density of the incompressible fluid flow. The superscript (d) denotes that the quantity is *dimensional* or of the *global* reference frame. All quantities in this section are assumed to have been non-dimensionalized with respect to the above scaling parameters unless otherwise indicated.

Let $\Psi(x, z)$ denote the stream function of the basic flow field. The basic flow field is perturbed by a small disturbance of frequency ω having a stream function of the form $\psi(x, z)\, e^{-i\omega t}$. The stream function of the disturbed flow $\Psi^T(x, z, t) = \Psi(x, z) + \psi(x, z)\, e^{-i\omega t}$ must necessarily satisfy the Navier–Stokes equations. By substituting Ψ^T into the Navier–Stokes equations, subtracting out the basic flow components and keeping only terms which are linear in ψ, we obtain

$$-i\omega(\nabla^2\psi) + \frac{\partial\Psi}{\partial z}\frac{\partial(\nabla^2\psi)}{\partial x} + \frac{\partial(\nabla^2\Psi)}{\partial x}\frac{\partial\psi}{\partial z} - \frac{\partial\Psi}{\partial x}\frac{\partial(\nabla^2\psi)}{\partial z} - \frac{\partial(\nabla^2\Psi)}{\partial z}\frac{\partial\psi}{\partial x} = \frac{1}{R_\delta}\nabla^4\psi, \tag{2.1}$$

where ∇^2 is the Laplacian in x and z and $R_\delta = U_\infty^{(d)}\delta_r^{(d)}\rho_f^{(d)}/\mu_f^{(d)}$ is the Reynolds number based on displacement thickness $\delta_r^{(d)}$. The disturbance ψ is coupled to a corresponding disturbance in the wall (see §2.3) and is assumed to decay to zero as $z \to \infty$.

The basic flow of interest here is the zero-pressure-gradient semi-infinite-plate boundary-layer whose stream function is given by

$$\Psi(x, z; R_\delta) = [m\epsilon(x_r + x)]^{1/2} f(\eta) + 0 \times \epsilon, \quad \eta = \frac{z}{[m\epsilon(x_r + x)]^{1/2}}, \tag{2.2}$$

where $x_r = x_r^{(d)}/\delta_r^{(d)}$, $\epsilon = m/R_\delta$ and $f(\eta)$ satisfies the Blasius equation

$$2f''' + m^2 f f'' = 0 \tag{2.3}$$

subject to the boundary conditions $f(0) = f'(0) = 0$ and $f'(\eta) \to 0$ as $\eta \to \infty$. The prime in (2.3) denotes an ordinary derivative with respect to η. A value of $m = 1.72078$, corresponding to $\eta = 1.0$ being the displacement thickness, is used here. It is noted that $\eta(x, z) = z$ along $x = 0$ because $m\epsilon x_r = 1$.

2.1.1. *Multiple-scale analysis for flow disturbances*

Boundary-layer non-parallelism arises from the variation of the basic stream function Ψ given by (2.2) with respect to the streamwise variable x. This variation is slow because $\epsilon = m/R_\delta$ is a small quantity in the R_δ range of interest. To apply a multiple-scale analysis, we introduce the two independent spatial variables $x_0 = x$ and $x_1 = \epsilon x$ and assume all the dependent variables to be functions of these spatial variables. The basic velocity field is then expanded as

$$U(x, z) = \partial_z \Psi(x_1, z) = U_0(x_1, z) + \epsilon U_1(x_1, z) + \ldots, \tag{2.4a}$$

$$W(x, z) = -\partial_x \Psi(x_1, z) = \epsilon W_1(x_1, z) + \ldots, \tag{2.4b}$$

where $U_0 = f'(\eta)$, $U_1 \equiv 0$ and $W_1 = \frac{1}{2}\left(\frac{m}{\epsilon x_r + x_1}\right)^{1/2}(\eta f' - f)$.

The disturbance stream function $\psi(x, z)$ is expanded as

$$\psi(x, z) = \psi_0(x_0, x_1, z) + \epsilon\psi_1(x_0, x_1, z) \ldots . \tag{2.5}$$

We note that ∂_x is equivalent to $\partial_{x_0} + \epsilon\partial_{x_1}$. The substitution of (2.4) and (2.5) into the governing equation (2.1) yields

$$O(\epsilon^0): \quad \mathscr{L}^f\psi_0 \equiv [(U_0\partial_{x_0} - \mathrm{i}\omega)\nabla_0^2 - (\partial_z^2 U_0)\partial_{x_0} - \nabla_0^4/R_\delta]\psi_0 = 0, \tag{2.6a}$$

$$\begin{aligned} O(\epsilon^1): \quad \mathscr{L}^f\psi_1 = {} & [U_0\partial_{x_1} + W_1\partial_z - R_\delta^{-1}(\partial_{x_0}\partial_{x_1} + \partial_{x_1}\partial_{x_0})]\nabla_0^2\psi_0 \\ & + [-\mathrm{i}\omega + U_0\partial_{x_0} - R_\delta^{-1}\nabla_0^2](\partial_{x_0}\partial_{x_1} + \partial_{x_1}\partial_{x_0})\psi_0 \\ & - [(\partial_z^2 W_1)\partial_z + (\partial_z^2 U_0)\partial_{x_1}]\psi_0, \end{aligned} \tag{2.6b}$$

where $\nabla_0^2 \equiv (\partial_{x_0}^2 + \partial_z^2)$. Equation (2.6*a*) is a linear partial differential equation in x_0 and z whose coefficients are either constant or depend on z through the velocity profile U_0. It admits a separable solution of the form $\psi_0 = A_0^f\phi_0(z)\exp(\mathrm{i}\alpha_0 x_0)$ where A_0^f is a quantity characterizing the amplitude of the disturbance. However, if we take into account the fact that U_0 has a slow dependence on x_1, then the global form of ψ_0 reflecting this dependence is

$$\psi_0(x_0, x_1, z) = A_0^f(x_1)\phi_0(x_1, z)\exp\left[\mathrm{i}\int_0^{x_0}\alpha_0(x_1)\,\mathrm{d}x_0\right], \tag{2.7}$$

wherein the amplitude A_0^f, function ϕ_0 and wavenumber α_0 are now dependent on the slow variable x_1. This is the spatial form of the disturbances considered by Gaster (1974) and Saric & Nayfeh (1975). The $O(\epsilon^1)$ equation (2.6*b*) is identical to the $O(\epsilon^0)$ equation (2.6*a*) when the inhomogeneous terms on its right-hand side are set to zero. We therefore assume ψ_1 to have the same form of solution:

$$\psi_1(x_0, x_1, z) = A_1^f(x_1)\phi_1(x_1, z)\exp\left[\mathrm{i}\int_0^{x_0}\alpha_0(x_1)\,\mathrm{d}x_0\right]. \tag{2.8}$$

Substituting (2.7) and (2.8) for ψ_0 and ψ_1 into (2.6), yields

$$\begin{aligned} O(\epsilon^0): \quad A_0^f L^f\phi_0 \equiv {} & [(U_0 - \omega/\alpha_0)(\partial_z^2 - \alpha_0^2) - (\partial_z^2 U_0) \\ & - (\mathrm{i}\alpha_0 R_\delta)^{-1}(\partial_z^4 - 2\alpha_0^2\partial_z^2 + \alpha_0^4)]A_0^f\phi_0 = 0, \end{aligned} \tag{2.9a}$$

$$O(\epsilon^1): \quad A_1^f L^f\phi_1 = F_1 A_0^f + F_2\partial_{x_1}A_0^f, \tag{2.9b}$$

where F_1 and F_2 are functions of x_1 and z given in the Appendix. The L^f in (2.9) is just the Orr–Sommerfeld operator and (2.9*a*) is the well-known Orr–Sommerfeld equation for the case of a locally parallel flow.

2.1.2. *The far-field boundary conditions*

The flow disturbance functions ϕ_0 and ϕ_1 are subjected to two sets of boundary conditions. One set pertains to the interaction between the disturbed flow and the compliant wall at their interface. This is considered in §2.3. The other set concerns the behaviour of the disturbance functions far away from the wall. Far away from the wall, the non-zero $O(\epsilon^0)$ and $O(\epsilon^1)$ basic flow components U_0 and W_1 tend to the constants 1.0 and 0.86039 respectively. Equation (2.9*a*) governing ϕ_0 then reduces to the constant-coefficient ordinary differential equation

$$L_\infty^f\phi_0 = [(\partial_z^2 - \alpha_0^2)(\partial_z^2 - \chi_0^2)]\phi_0 = 0, \tag{2.10}$$

where $\chi_0 = [\alpha_0^2 + \mathrm{i}R_\delta(\alpha_0 - \omega)]^{1/2}$, which has simple exponential solutions. Since admissible flow disturbances must clearly decay to zero as z tends to ∞, this implies that the solution for ϕ_0 far away from the wall must have the form

$$\phi_0(x_1, z) = C_{0\alpha}(x_1)\,\mathrm{e}^{-\alpha_0 z} + C_{0\chi}(x_1)\,\mathrm{e}^{-\chi_0 z}, \tag{2.11}$$

where $\mathrm{Re}(\alpha_0) > 0$, $\mathrm{Re}(\chi_0) > 0$. The corresponding far-field condition for the $O(\epsilon^1)$ disturbance function $\phi_1(x_1, z)$ is

$$L_\infty^f \phi_1 = (L_1 + L_2 z)\,\mathrm{e}^{-\alpha_0 z} + (L_3 + L_4 z)\,\mathrm{e}^{-\chi_0 z}, \tag{2.12}$$

where the right-hand-side terms are derived from the far-field solution of ϕ_0 given by (2.11). Equation (2.12) is a non-homogeneous equation whose solution has the form

$$\phi_1(x_1, z) = C_{1\alpha}\,\mathrm{e}^{-\alpha_0 z} + C_{1\chi}\,\mathrm{e}^{-\chi_0 z} + (H_1 z + H_2 z^2)\,\mathrm{e}^{-\alpha_0 z} + (H_3 z + H_4 z^2)\,\mathrm{e}^{-\chi_0 z}, \tag{2.13}$$

where the last two terms on the right-hand side correspond to the particular integral. By eliminating the coefficients $C_{0\alpha}$, $C_{0\chi}$, $C_{1\alpha}$ and $C_{1\chi}$ from the solutions of ϕ_0 and ϕ_1 respectively, on the assumption that ϕ_0 and ϕ_1 are sufficiently differentiable, the following equations are obtained for ϕ_0 and ϕ_1 in the far field:

$$\boldsymbol{M}_\infty \boldsymbol{\phi}_0 = \boldsymbol{0}, \tag{2.14a}$$

$$\boldsymbol{M}_\infty \boldsymbol{\phi}_1 = \boldsymbol{\gamma}_\infty = \boldsymbol{\gamma}_{\infty 1} A_0^f + \boldsymbol{\gamma}_{\infty 2}\,\partial_{x_1} A_0^f, \tag{2.14b}$$

where

$$\boldsymbol{M}_\infty = \begin{bmatrix} \alpha_0\chi_0 & \alpha_0 + \chi_0 & 1 & 0 \\ 0 & \alpha_0\chi_0 & \alpha_0 + \chi_0 & 1 \end{bmatrix},$$

$$\boldsymbol{\phi}_0 = (\phi_0, \phi_0', \phi_0'', \phi_0''')^T \quad \text{and} \quad \boldsymbol{\phi}_1 = (\phi_1, \phi_1', \phi_1'', \phi_1''')^T.$$

The prime refers to a derivative with respect to z. $\boldsymbol{\gamma}_{\infty 1}$ and $\boldsymbol{\gamma}_{\infty 2}$ are 2-vectors.† In this study, the boundary conditions (2.14) for the flow disturbance functions ϕ_0 and ϕ_1 are implemented at large values of z, denoted by z_∞, ranging from 6 to 8 displacement thicknesses.

2.2. *Dynamics of a compliant layer*

In this section, the equations governing wall disturbances in a single-layer compliant wall at $O(\epsilon^0)$ and $O(\epsilon^1)$ are derived and solved. The layer is assumed to be homogeneous, isotropic and uniformly thick. The non-dimensionalization of the wall quantities follows that for the flow domain except for the lengthscale, where a fixed wall lengthscale denoted by $L_w^{(d)}$, instead of the local lengthscale $\delta_r^{(d)}$, is used (see Yeo 1988).

The dynamics of a small-amplitude sinusoidal displacement wave field $\boldsymbol{h}(x, z, t) = \boldsymbol{\eta}(x, z)\,\mathrm{e}^{-\mathrm{i}\omega t}$ in the compliant layer (in the absence of mean-state interaction and body forces) is governed by the following viscoelastic analogue of Navier's equations:

$$-\rho\omega^2\boldsymbol{\eta} = \tfrac{1}{2}Y_s\nabla^2\boldsymbol{\eta} + \tfrac{1}{6}(2Y_v + Y_s)\,\boldsymbol{\nabla}\boldsymbol{\nabla}\cdot\boldsymbol{\eta}, \tag{2.15}$$

where $\boldsymbol{\eta} = (\eta_x, \eta_z)^T$ is the spatial part of the displacement field associated with the disturbance, defined with reference to a suitable Lagrangian reference state. The reference state may be taken to be the state of the wall that is in static equilibrium with the basic flow. $\boldsymbol{\nabla}$ is the gradient operator, and Y_s and Y_v are the deviatoric and dilatational complex moduli respectively (see Bland 1960). As in Yeo (1988), we assume the behaviour of the materials to obey a Voigt-type damping model in shear and to be elastic in isotropic deformation. The complex moduli Y_s and Y_v are related to the more familiar bulk modulus K (real in this case) and shear modulus G by

$$Y_s = 2G = 2(\rho C_t^2 - \mathrm{i}\omega d) \quad \text{and} \quad Y_v = 3K, \tag{2.16a, b}$$

† The details for the 2-vectors $\boldsymbol{\gamma}_{\infty 1}$ and $\boldsymbol{\gamma}_{\infty 2}$ and the functions H_i and L_i ($i = 1, \ldots, 4$) may be obtained from the authors or the JFM editorial office.

where C_t is the material's elastic shear wave speed, and d the damping coefficient. The disturbance stresses in the wall are given by the linear isotropic stress-strain law

$$\sigma_{xx} = (\lambda+2G)e_{xx}+\lambda e_{zz}, \quad \sigma_{zz} = (\lambda+2G)e_{zz}+\lambda e_{xx}, \quad \sigma_{zx} = 2Ge_{zx}, \quad (2.17a\text{–}c)$$

where $\lambda = K-\frac{2}{3}G$, and e_{xx}, e_{zz}, and e_{zx} are the linear strains. Navier's equation (2.15) and the stress-strain relation (2.17) can be reformulated into the following useful first-order form:

$$\partial_z \boldsymbol{S} = \boldsymbol{B}\boldsymbol{S} \quad (2.18)$$

involving the displacement-stress vector $\boldsymbol{S} = (\eta_x, \eta_z, \sigma_{zx}, \sigma_{zz})^T$ used by Yeo (1988), where

$$\boldsymbol{B} = \begin{bmatrix} 0 & -\partial_x & G^{-1} & 0 \\ -\lambda(\lambda+2G)^{-1}\partial_x & 0 & 0 & (\lambda+2G)^{-1} \\ -\rho\omega^2+4G(\lambda+G)(\lambda+2G)^{-1}\partial_x^2 & 0 & 0 & -\lambda(\lambda+2G)^{-1}\partial_x \\ 0 & -\rho\omega^2 & -\partial_x & 0 \end{bmatrix}.$$

2.2.1. *Multiple-scale analysis of wall dynamics*

In applying the multiple-scale analysis, we expand the displacement components η_x and η_z, and the stress components σ_{zx} and σ_{zz} as series in ϵ as follows:

$$\eta_x = \eta_{x0}(x_0, x_1, z)+\epsilon\eta_{x1}(x_0, x_1, z)+\ldots, \quad (2.19a)$$

$$\eta_z = \eta_{z0}(x_0, x_1, z)+\epsilon\eta_{z1}(x_0, x_1, z)+\ldots, \quad (2.19b)$$

$$\sigma_{zx} = \sigma_{zx0}(x_0, x_1, z)+\epsilon\sigma_{zx1}(x_0, x_1, z)+\ldots, \quad (2.19c)$$

$$\sigma_{zz} = \sigma_{zz0}(x_0, x_1, z)+\epsilon\sigma_{zz1}(x_0, x_1, z)+\ldots, \quad (2.19d)$$

and write the displacement-stress vector $\boldsymbol{S}$ as

$$\boldsymbol{S}(x, z) = \boldsymbol{S}_0(x_0, x_1, z)+\epsilon\boldsymbol{S}_1(x_0, x_1, z)+\ldots, \quad (2.20)$$

where $\boldsymbol{S}_j = (\eta_{xj}, \eta_{zj}, \sigma_{zxj}, \sigma_{zzj})^T$. For consistency with the solutions of the flow domain, we expect the $\boldsymbol{S}_j$ ($j = 0, 1, \ldots$) to possess factorized spatial wave solutions of the form

$$\boldsymbol{S}_j(x_0, x_1, z) = A_j^w(x_1)\,\hat{\boldsymbol{S}}_j(x_1, z)\exp\left[\mathrm{i}\int_0^{x_0}\alpha_0(x_1)\,\mathrm{d}x_0\right], \quad (2.21)$$

where $\hat{\boldsymbol{S}}_j(x_1, z) = (\hat{\eta}_{xj}, \hat{\eta}_{zj}, \hat{\sigma}_{zxj}, \hat{\sigma}_{zzj})^T$. The substitution of (2.20) and (2.21) into equation (2.18) and expanding ∂_x as $\partial_x+\epsilon\partial_{x_1}$ result in two equations for the amplitude functions $\hat{\boldsymbol{S}}_0$ and $\hat{\boldsymbol{S}}_1$:

$$O(\epsilon^0): \quad A_0^w\,\mathscr{L}^w\hat{\boldsymbol{S}}_0 \equiv [\partial_z-\boldsymbol{C}_0]A_0^w\hat{\boldsymbol{S}}_0 = 0, \quad (2.22a)$$

$$O(\epsilon^1): \quad A_1^w\,\mathscr{L}^w\hat{\boldsymbol{S}}_1 = \boldsymbol{C}_1 A_0^w\hat{\boldsymbol{S}}_0+\boldsymbol{C}_2\partial_{x_1}(A_0^w\hat{\boldsymbol{S}}_0), \quad (2.22b)$$

where $\boldsymbol{C}_0$, $\boldsymbol{C}_1$ and $\boldsymbol{C}_2$, listed in the Appendix, are matrix functions of material properties. For a homogeneous layer, these are constant matrices.

2.2.2. *Solution of the wall perturbation equations*

Equations (2.22a, b) are systems of first-order linear ordinary differential equations for $\hat{\boldsymbol{S}}_0$ and $\hat{\boldsymbol{S}}_1$ respectively regarded as a function of z. Equation (2.22b) is non-homogeneous with right-hand side determined by the solution for $\hat{\boldsymbol{S}}_0$. We are interested in the solutions of (2.22a, b) which relate the values of $\boldsymbol{S}_0$ and $\boldsymbol{S}_1$ at two points, say z_a and z_b, within the compliant layer. The compliant layer has its top and bottom surfaces at $z = z_0$ and at $z = z_1$ respectively. The solution to (2.22a) for $\hat{\boldsymbol{S}}_0$ is

$$\hat{\boldsymbol{S}}_0(z_b) = \boldsymbol{P}(z_b, z_a)\,\hat{\boldsymbol{S}}_0(z_a) \quad (z_1 \leqslant z_a, z_b \leqslant z_0), \quad (2.23)$$

where $\boldsymbol{P}(z_b, z_a)$ is the exponential matrix $\exp[(z_b-z_a)\boldsymbol{C}_0]$. The two-argument matrix

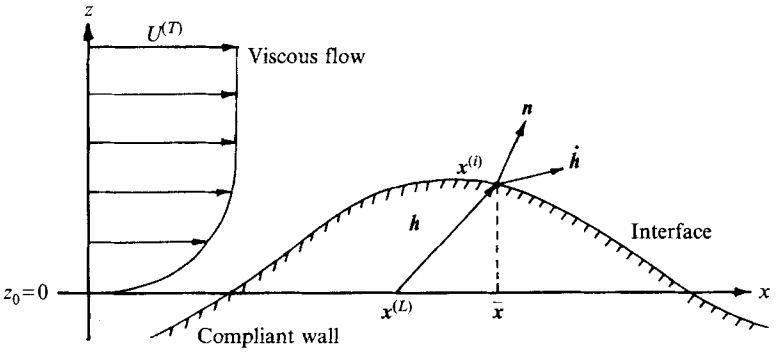

FIGURE 2. Flow–wall interface. $\bar{\boldsymbol{x}} = (x, z_0)$; $\boldsymbol{x}^{(i)} = (x, z_0 + h_z)$, coordinate of interface; $\boldsymbol{x}^{(L)} = (x^L, z_0)$, material coordinate of $\boldsymbol{x}^{(i)}$.

function $\boldsymbol{P}(z_b, z_a)$ is termed the *propagation matrix*. The solution of (2.22 *b*) for $\hat{\boldsymbol{S}}_1$ is given by

$$A_1^w \hat{\boldsymbol{S}}_1(z_b) = \boldsymbol{P}(z_b, z_a) A_1^w \hat{\boldsymbol{S}}_1(z_a) + \int_{z_a}^{z_b} \boldsymbol{P}(z_b, \xi) [\boldsymbol{C}_1 A_0^w \hat{\boldsymbol{S}}_0(\xi) + \boldsymbol{C}_2 \partial_{x_1}(A_0^w \hat{\boldsymbol{S}}_0(\xi))] \, \mathrm{d}\xi \quad (2.24)$$

for z_a and z_b in the layer; see Coddington & Levinson (1955) or Gilbert & Backus (1966). The solution (2.24) may be further developed by noting that the term $\partial_{x_1}(A_0^w \hat{\boldsymbol{S}}_0(\xi))$ under the integral satisfies an equation similar to (2.22*b*). Its solution allows us to rewrite (2.24) as

$$A_1^w \hat{\boldsymbol{S}}_1(z_b) = \boldsymbol{P}(z_b, z_a) A_1^w \hat{\boldsymbol{S}}_1(z_a) + \int_{z_a}^{z_b} \boldsymbol{P}(z_b, \xi) [\boldsymbol{C}_2 \boldsymbol{G}_1(\xi) + \boldsymbol{C}_1 \boldsymbol{P}(\xi, z_a) A_0^w \hat{\boldsymbol{S}}_0(z_a)] \, \mathrm{d}\xi$$
$$+ \int_{z_a}^{z_b} \boldsymbol{P}(z_b, \xi) \boldsymbol{C}_2 \boldsymbol{P}(\xi, z_a) \partial_{x_1}(A_0^w \hat{\boldsymbol{S}}_0(z_a)) \, \mathrm{d}\xi, \quad (2.25)$$

where $$\boldsymbol{G}_1(\xi) = \int_{z_a}^{\xi} \boldsymbol{P}(\xi, \vartheta) \boldsymbol{F}_1(\vartheta) \boldsymbol{P}(\vartheta, z_a) A_0^w \hat{\boldsymbol{S}}_0(z_a) \, \mathrm{d}\vartheta.$$

Matrix $\boldsymbol{F}_1$ is given in the Appendix. Compared with (2.24), (2.25) only involves the value of $\partial_{x_1}(A_0^w \hat{\boldsymbol{S}}_0)$ at a fixed point z_a. The solution (2.23) and (2.25) for $\hat{\boldsymbol{S}}_0$ and $\hat{\boldsymbol{S}}_1$ are combined with the flow–wall interface boundary conditions in the next section to produce the necessary boundary conditions for the disturbance flow functions ϕ_0 and ϕ_1.

2.3. *The coupling of fluid and wall perturbations*

Having established the essential dynamics of the flow and the wall, it remains to consider their coupling at the interface, which has a mean and 'undisturbed' position along $z = z_0$. This is carried out below in §2.3.1, where the interface boundary conditions applicable to the interactions at $O(\epsilon^0)$ and $O(\epsilon^1)$ are derived. In §2.3.2, the interface boundary conditions are combined with the wall solutions of §2.2.2 to produce the necessary wall boundary conditions for the flow functions ϕ_0 and ϕ_1. The wall reference lengthscale $L_w^{(d)}$ is employed throughout this section unless otherwise indicated.

2.3.1. *The interface boundary conditions*

Figure 2 shows a schematic view of the flow–wall interface with greatly exaggerated wave amplitude. The total velocity of the flow field is $\boldsymbol{U}^{(T)} = (U+u, W+w)$, where $(u, w) = (\partial_z, -\partial_x)\psi \, \mathrm{e}^{-\mathrm{i}\omega t}$ denotes the perturbation component. $\boldsymbol{x}^{(L)} = (x^L, z_0)$ denotes

the mean (undisturbed) position of the interface points with respect to an appropriate Lagrangian reference frame. The interface points are moved by the perturbation displacement field $\boldsymbol{h} = (h_x, h_z) = (\eta_x, \eta_z)\,\mathrm{e}^{-\mathrm{i}\omega t}$ to $\boldsymbol{x}^{(i)} = \boldsymbol{x}^{(L)} + \boldsymbol{h} = (x, z_0 + h_z)$. The coupling of flow and wall motions is provided by the kinematic and the dynamical interface boundary conditions:

(i) the continuity of velocity at the interface

$$\dot{\boldsymbol{h}}|_{\boldsymbol{x}^{(L)}} = \boldsymbol{U}^{(T)}|_{\boldsymbol{x}^{(i)}}, \tag{2.26}$$

(iii) and the continuity of surface traction at the interface

$$\sigma_{jk}^{(T)}|_{\boldsymbol{x}^{(L)}}\, n_k = \sigma_{jk}^{f(T)}|_{\boldsymbol{x}^{(i)}}\, n_k, \tag{2.27}$$

where the subscript indices j, k range over the coordinate indices x and z. $\boldsymbol{n} = (n_x, n_z)$ is the instantaneous normal to the surface at $\boldsymbol{x}^i$. Superscript (T) denotes the total of the basic (or mean) and the perturbation quantities. The total Cartesian flow stresses are given by

$$\sigma_{jk}^{f(T)} = -p^{(T)}\,\delta_{jk} + \frac{1}{R_w}(U_{j,k}^{(T)} + U_{k,j}^{(T)}), \tag{2.28}$$

where $R_w = U_\infty^{(d)} L_w^{(d)} \rho_f^{(d)} / \mu_f^{(d)}$ is the Reynolds number based on wall lengthscale and $p^{(T)}$ is the total pressure field which can be calculated from the Navier–Stokes equations.

The flow–wall coupling conditions (2.26) and (2.27) are approximated at the mean position of the interface through Taylor expansion about $\bar{\boldsymbol{x}} = (x, z_0)$. The Taylor expansion of (2.26) about $\bar{\boldsymbol{x}}$, keeping only terms up to first order in disturbance quantities, yields

$$-\mathrm{i}\omega\eta_x = \partial_z \psi + \eta_z(\partial_z U), \quad -\mathrm{i}\omega\eta_z = -\partial_x \psi, \tag{2.29a, b}$$

where all the terms are evaluated at mean interface point $\bar{\boldsymbol{x}}$. Similar Taylor expansion of the dynamical interface condition (2.27), noting that the total stresses are sums of mean (overbar) and perturbation stresses, yields

$$\bar{\sigma}_{jk}\, n_k - \eta_x \left[\frac{\partial \bar{\sigma}_{jk}}{\partial x^{(L)}}\right] n_k + \sigma_{jk}\, n_k = \bar{\sigma}_{jk}^f\, n_k + \eta_z \left[\frac{\partial \bar{\sigma}_{jk}^f}{\partial z}\right] n_k + \sigma_{jk}^f\, n_k \quad (j,k = x,z), \tag{2.30}$$

where all the terms are evaluated at $\bar{\boldsymbol{x}}$. Taking into account that in the mean (undisturbed) state $\bar{\sigma}_{zx} = \bar{\sigma}_{zx}^f$ and $\bar{\sigma}_{zz} = \bar{\sigma}_{zz}^f$ at the mean interface $\bar{\boldsymbol{x}}$ and that $\partial_{x^{(L)}} = \partial_x$ to within the linearization approximation, equation (2.30) simplifies to

$$\sigma_{zx} = \sigma_{zx}^f + \frac{1}{R_w}\eta_x(\partial_x \partial_z U), \quad \sigma_{zz} = \sigma_{zz}^f - \frac{1}{R_w}\eta_z(\partial_x \partial_z U). \tag{2.31a, b}$$

A term equal to $(\bar{\sigma}_{xx} - \bar{\sigma}_{xx}^f)\,\partial_x \eta_z$ has been omitted from the right-hand side of (2.31 *a*). $\bar{\sigma}_{xx}$ need not be equal to $\bar{\sigma}_{xx}^f$ when there is non-zero pressure loading on the wall. Similar terms also exist for interaction between adjacent solid layers of different materials. To take these terms into account, mean pressure loading on the surface has to be specified, see Yeo, Khoo & Chong (1992, 1994). In this paper we neglected the effect of mean-pressure loading so that these terms are zero.

We can now apply multiple-scale analysis to the interface boundary conditions (2.29) and (2.31) by expanding $\sigma_{jk} = \sigma_{jk0} + \epsilon\sigma_{jk1}$, $\eta_x = \eta_{x0} + \epsilon\eta_{x1}$, $\eta_z = \eta_{z0} + \epsilon\eta_{z1}$, and $\partial_x = \partial_{x_0} + \epsilon\partial_{x_1}$ as in the preceding section. The perturbation flow stresses σ_{zx}^f and σ_{zz}^f are expanded in terms of flow eigenfunctions ϕ_0 and ϕ_1 via (2.28). The analysis yields the following equations, in matrix form, which couple the $O(\epsilon^0)$ and $O(\epsilon^1)$ displacement-

stress vectors $\hat{\boldsymbol{S}}_0$ and $\hat{\boldsymbol{S}}_1$ of the wall at z_0 (mean interface) to the flow eigenfunctions, ϕ_0 and ϕ_1, and their derivatives at the same point:

$$O(\epsilon^0): \qquad A_0^w \boldsymbol{S}_0(z_0) = \boldsymbol{Q}_c(z_0)\, A_0^f \boldsymbol{\phi}_0(z_0), \tag{2.32a}$$

$$O(\epsilon^1): \qquad A_1^w \hat{\boldsymbol{S}}_1(z_0) = \boldsymbol{Q}_c(z_0)\, A_1^f \boldsymbol{\phi}_1(z_0) + \boldsymbol{D}_1\, A_0^f \boldsymbol{\phi}_0(z_0) + \boldsymbol{D}_2\, \partial_{x_1}(A_0^f \boldsymbol{\phi}_0(z_0)), \tag{2.32b}$$

where the matrices $\boldsymbol{Q}_c, \boldsymbol{D}_1$ and $\boldsymbol{D}_2$ are given in the Appendix. The $O(\epsilon^0)$ equation (2.32*a*) is equivalent to the matrix interface boundary condition that has been used in Yeo (1986, 1988) in his study of the locally parallel flow case.

2.3.2. *Wall boundary conditions for ϕ_0 and ϕ_1*

The wall boundary conditions for the flow functions ϕ_0 and ϕ_1 may now be obtained by combining the interface boundary conditions (2.32) above with the solutions for the wall (2.23) and (2.25). Before doing that, we note that the term $\partial_{x_1}(A_0^w \hat{\boldsymbol{S}}_0)$ in (2.25) (with z_a now replaced by z_0) may be obtained in terms of ϕ_0 and ϕ_1 at z_0 through the differentiation of (2.32*a*):

$$\partial_{x_1}(A_0^w \hat{\boldsymbol{S}}_0(z_0)) = \boldsymbol{Q}_c\, A_0^f\, \partial_{x_1} \boldsymbol{\phi}_0(z_0) + \boldsymbol{Q}_c \boldsymbol{\phi}_0\, \partial_{x_1} A_0^f + \boldsymbol{E}_1\, A_0^f \boldsymbol{\phi}_0(z_0) \tag{2.33}$$

(matrix $\boldsymbol{E}_1$ is given in the Appendix). We can now combine the interface conditions and the wall solutions by substituting (2.32) and (2.33) into (2.23) and (2.25) with z_a set to z_0 (the position of the mean flow–wall interface) and $z_b = z_1$ (the bottom of the compliant layer). The resultant equations are

$$O(\epsilon^0): \qquad A_0^w \hat{\boldsymbol{S}}_0(z_1) = \boldsymbol{P}(z_1, z_0)\, \boldsymbol{Q}_c\, A_0^f \boldsymbol{\phi}_0(z_0), \tag{2.34a}$$

$$O(\epsilon^1): \qquad A_1^w \hat{\boldsymbol{S}}_1(z_1) = \boldsymbol{P}(z_1, z_0)\, \boldsymbol{Q}_c\, A_1^w \boldsymbol{\phi}_1(z_0) - \gamma_{w1} A_0^f - \gamma_{w2}\, \partial_{x_1} A_0^f, \tag{2.34b}$$

where

$$\gamma_{w1} = -\boldsymbol{P}(z_1, z_0)[\boldsymbol{D}_1 \boldsymbol{\phi}_0(z_0) - \boldsymbol{D}_2\, \partial_{x_1} \boldsymbol{\phi}_0(z_0)] - \int_{z_0}^{z_1} \boldsymbol{P}(z_1, \xi)\, \boldsymbol{C}_2\, \boldsymbol{G}_2(\xi)\, \mathrm{d}\xi$$
$$- \int_{z_0}^{z_1} \boldsymbol{P}(z_1, \xi)\, \boldsymbol{C}_1\, \boldsymbol{P}(\xi, z_0)\, \boldsymbol{Q}_c \boldsymbol{\phi}_0(z_0)\, \mathrm{d}\xi, \tag{2.34c}$$

$$\gamma_{w2} = -\boldsymbol{P}(z_1, z_0)\, \boldsymbol{D}_2 \boldsymbol{\phi}_0(z_0) - \int_{z_0}^{z_1} \boldsymbol{P}(z_1, \xi)\, \boldsymbol{C}_2\, \boldsymbol{P}(\xi, z_0)\, \boldsymbol{Q}_c \boldsymbol{\phi}_0(z_0)\, \mathrm{d}\xi, \tag{2.34d}$$

and

$$\boldsymbol{G}_2(\xi) = \boldsymbol{P}(\xi, z_0)[\boldsymbol{Q}_c\, \partial_{x_1} \boldsymbol{\phi}_0(z_0) + \boldsymbol{E}_1 \boldsymbol{\phi}_0(z_0)] + \int_{z_0}^{\xi} \boldsymbol{P}(\xi, \vartheta)\, \boldsymbol{F}_1(\vartheta) \boldsymbol{P}(\vartheta, z_0)\, \boldsymbol{Q}_c \boldsymbol{\phi}_0(z_0)\, \mathrm{d}\vartheta.$$

Equations (2.34*a*, *b*) now relate the flow eigenfunctions $\boldsymbol{\phi}_0$ and $\boldsymbol{\phi}_1$ at the mean flow–wall interface at $z = z_0$ to the wall's displacement-stress vectors $\hat{\boldsymbol{S}}_0$ and $\hat{\boldsymbol{S}}_1$ at the bottom of the compliant layer at $z = z_1$. At this bottom interface, the displacement components $\eta_{x0}(z_1)$, $\eta_{z0}(z_1)$, $\eta_{x1}(z_1)$ and $\eta_{z1}(z_1)$ in $\hat{\boldsymbol{S}}_0$ and $\hat{\boldsymbol{S}}_1$ are zero because we have assumed perfect bonding between the compliant layer and the rigid base. With these, the required wall boundary conditions for $\boldsymbol{\phi}_0$ and $\boldsymbol{\phi}_1$ at $z = z_0$ are hence given by the first two rows of matrix equations (2.34*a*) and (2.34*b*), namely,

$$O(\epsilon^0): \qquad {}^2\boldsymbol{M}_w\, A_0^f \boldsymbol{\phi}_0(z_0) = \boldsymbol{0}_2, \tag{2.35a}$$

$$O(\epsilon^1): \qquad {}^2\boldsymbol{M}_w\, A_1^f \boldsymbol{\phi}_1(z_0) = {}^2\boldsymbol{\gamma}_w = {}^2\boldsymbol{\gamma}_{w1} A_0^f + {}^2\boldsymbol{\gamma}_{w2}\, \partial_{x1} A_0^f, \tag{2.35b}$$

where $$\boldsymbol{M}_w = \boldsymbol{P}(z_1, z_0)\, \boldsymbol{Q}_c\, \boldsymbol{M}_s.$$

$\boldsymbol{0}_2$ is the null 2-vector. The left superscript 2 is used here to denote the first two rows of the matrix or vector. The diagonal matrix $\boldsymbol{M}_s \equiv \mathrm{Diag}\{r, 1, r^{-1}, r^{-2}\}$ ($r = R_\delta / R_w$) is

added at this point to convert ϕ_0 and ϕ_1 (which has hitherto been interpreted in term of the wall lengthscale $L_w^{(a)}$ in this section) to the flow lengthscale $\delta_r^{*(a)}$, so that the wall boundary conditions (2.35) are compatible with the flow disturbance equations (2.9).

2.4. *The stability eigenvalue problem and correction for boundary-layer growth*

We have obtained by now all the equations that we need to specify our stability problem at $O(\epsilon^0)$ ((2.9*a*), (2.14*a*) and (2.35*a*)) and at $O(\epsilon^1)$ ((2.9*b*), (2.14*b*) and (2.35*b*)). We collect these together below for the convenience of subsequent reference.

$O(\epsilon^0)$: $$L^f\phi_0(z) = 0 \quad (z_0 < z < z_\infty), \tag{2.36a}$$

subject to $$^2\boldsymbol{M}_w\boldsymbol{\phi}_0(z_0) = \mathbf{0}_2, \quad \boldsymbol{M}_\infty\boldsymbol{\phi}_0(z_\infty) = \mathbf{0}_2 \tag{2.36b, c}$$

where the amplitude function $A_0^f(x_1)$, which does not affect the solution of $\boldsymbol{\phi}_0$, has been discarded.

$O(\epsilon^1)$: $$L^f\phi_1(z) = F_1 A_0^f + F_2\,\partial_{x_1} A_0^f \quad (z_0 < z < z_\infty), \tag{2.37a}$$

subject to $$^2\boldsymbol{M}_w\boldsymbol{\phi}_1(z_0) = {}^2\boldsymbol{\gamma}_w = {}^2\boldsymbol{\gamma}_{w1} A_0^f + {}^2\boldsymbol{\gamma}_{w2}\,\partial_{x_1} A_0^f, \tag{2.37b}$$

$$\boldsymbol{M}_\infty\boldsymbol{\phi}_1(z_\infty) = \boldsymbol{\gamma}_\infty = \boldsymbol{\gamma}_{\infty 1} A_0^f + \boldsymbol{\gamma}_{\infty 2}\,\partial_{x_1} A_0^f. \tag{2.37c}$$

The amplitude function $A_1^f(x_1)$ does not affect the solution we seek and has also been removed from (2.37).

The system of equations (2.36) for the $O(\epsilon^0)$ problem represents the stability eigenvalue problem for the boundary layer treated as a locally parallel flow (Yeo 1988), as only the x-component of the basic flow U and its derivative with respect to z are involved in its formulation. For specified Reynolds number R_δ and frequency ω (taken to be real in this study), non-trivial solutions ϕ_0 exist only for certain values of the streamwise wavenumber α_0. In the locally parallel context, there is instability when $\mathrm{Im}(\alpha_0) < 0$. corresponding to a downstream growing wave.

The differential and boundary operators of the $O(\epsilon^1)$ problem (2.37) are identical to those for (2.36). System (2.37) differs from (2.36) because of the presence of non-homogeneous terms on its right-hand side representing the influence of flow-non-parallelism. The $O(\epsilon^1)$ problem has a solution ϕ_1 provided the solvability condition

$$\int_0^{z_\infty} (F_1 A_0^f + F_2\,\partial_{x_1} A_0^f)\varphi^*\,\mathrm{d}z = \begin{pmatrix} {}^2\boldsymbol{\gamma}_w \\ \boldsymbol{\gamma}_\infty \end{pmatrix} \cdot \boldsymbol{U}_{BC}^+ \begin{pmatrix} \boldsymbol{\varphi}(z_0) \\ \boldsymbol{\varphi}(z_\infty) \end{pmatrix} \tag{2.38}$$

holds for every solution of $\varphi(z)$ of the adjoint homogeneous problem to system (2.37); $\boldsymbol{\varphi} \equiv (\varphi, \varphi', \varphi'', \varphi''')^T$. Superscript asterisk denotes complex conjugation and the centre-dot product is the complex inner product. $\boldsymbol{U}_{BC}^+$ is the 4×8 matrix termed the complementary adjoint boundary matrix.† We note that the homogeneous adjoint problem of (2.37) is identical to the homogeneous adjoint of (2.36) and they have the same eigenvalues α_0 as the original eigenvalue problem (2.36). The more complex form of the solvability condition (2.38), compared to that used by Gaster (1974) and others, arises from the presence of derivative boundary conditions at both $z = 0$ and z_∞ (set to 6 or 8). The matrix $\boldsymbol{U}_{BC}^+$ has the two-point separated form

$$\boldsymbol{U}_{BC}^+ = \begin{bmatrix} \boldsymbol{M}_{wc}^+ & \mathbf{0}_{2\times 4} \\ \mathbf{0}_{2\times 4} & \boldsymbol{M}_{\infty c}^+ \end{bmatrix}$$

so that expanding (2.38) yields

$$\frac{\mathrm{d}A_0^f}{\mathrm{d}x_1} = \mathrm{i}\alpha_1(x_1)\,A_0^f, \tag{2.39}$$

† The details concerning the derivation of the solvability condition and the associated complementary adjoint boundary matrix may be obtained from the authors or the JFM editorial office.

where $$\mathrm{i}\alpha_1(x_1) = -\frac{(J_1 - \gamma_{\infty 1}\cdot \boldsymbol{M}^+_{\infty c}\boldsymbol{\varphi}(z_\infty) - {}^2\gamma_{w1}\cdot \boldsymbol{M}^+_{wc}\boldsymbol{\varphi}(z_0))}{(J_2 - \gamma_{\infty 2}\cdot \boldsymbol{M}^+_{\infty c}\boldsymbol{\varphi}(z_\infty) - {}^2\gamma_{w2}\cdot \boldsymbol{M}^+_{wc}\boldsymbol{\varphi}(z_0))},$$

$$J_1 = \int_0^{z_\infty} F_1 \varphi^* \,\mathrm{d}z \quad \text{and} \quad J_2 = \int_0^{z_\infty} F_2 \varphi^* \,\mathrm{d}z.$$

The solution of the locally parallel eigenvalue problem (2.36) and the evaluation of (2.39), which gives the x_1-variation of A_0^f, together fully specifies the $O(\epsilon^0)$ disturbance stream function ψ_0 given in (2.7) up to an arbitrary constant. By differentiating ψ_0 with respect to x and using (2.39), we have

$$\partial_x \psi_0|_{x=0} = \alpha_{\varphi}(z; R_\delta)\,\psi_0|_{x=0}, \tag{2.40a}$$

where $$\alpha_{\varphi}(z; R_\delta) = [\mathrm{i}\alpha_0 + \epsilon(\mathrm{i}\alpha_1 + \phi_0^{-1}\partial_{x_1}\phi_0)]_{x=0}. \tag{2.40b}$$

Equation (2.40) describes the streamwise rate of change of the $O(\epsilon^0)$ disturbance stream function ψ_0 with respect to the local Cartesian frame (x, z) at the streamwise location of Reynolds number R_δ. The influence of boundary-layer non-parallelism is contained in the term $\epsilon(\mathrm{i}\alpha_1 + \phi_0^{-1}\partial_{x_1}\phi_0)$ which is asymptotically small at large R_δ since $\epsilon = mR_\delta^{-1}$.

The downstream spatial growth rate of the locally parallel flow theory is $-\mathrm{Im}\,(\alpha_0)$ for first-degree disturbance quantities and $-2\,\mathrm{Im}\,(\alpha_0)$ for quadratic disturbance quantities. Non-parallel corrections to $O(\epsilon^1)$ may be determined from the solution of (2.36) and the evaluation of (2.39). The $O(\epsilon^1)$ corrections are generally different for different physical quantities. The spatial growth rates of the following physical quantities have been considered in the literature:

(*a*) the kinetic energy integral

$$E(x) = \int_0^\infty (\overline{u^2} + \overline{w^2})\,\mathrm{d}z, \tag{2.41}$$

(*b*) the $|u|^2$ integral

$$I(x) = \int_0^\infty (\overline{u^2})\,\mathrm{d}z, \tag{2.42}$$

(*c*) the horizontal and vertical root-mean-square perturbation velocities

$$|u| = (\overline{u^2})^{1/2}, \quad |w| = (\overline{w^2})^{1/2}, \tag{2.43a, b}$$

where $u = \mathrm{Re}\,(\partial_z \psi_0\, \mathrm{e}^{-\mathrm{i}\omega t})$ and $w = -\mathrm{Re}\,(\partial_x \psi_0\, \mathrm{e}^{-\mathrm{i}\omega t})$ are the horizontal and vertical components of the perturbation velocity respectively. The overbar here denotes time averaging. The quantities $\overline{u^2}$, $\overline{w^2}$ and $\overline{u^2}+\overline{w^2}$ can be measured using hot-wire anemometry. Employing (2.39), it is not difficult to show that the downstream amplification rates for $E(x)$, $I(x)$, $|u|$ and $|w|$ to $O(\epsilon^1)$ are given by

$$\alpha^{(E)} = \frac{1}{E}\frac{\mathrm{d}E}{\mathrm{d}x} = -2\,\mathrm{Im}\,(\alpha_0 + \epsilon\alpha_1) + \epsilon\left\{\frac{1}{e}\partial_{x_1} e\right\}, \tag{2.44}$$

$$\alpha^{(I)} = \frac{1}{I}\frac{\mathrm{d}I}{\mathrm{d}x} = -2\,\mathrm{Im}\,(\alpha_0 + \epsilon\alpha_1) + \epsilon\left\{\frac{1}{\mathscr{k}}\partial_{x_1}\mathscr{k}\right\}, \tag{2.45}$$

where $$e = \int_0^\infty (\phi_0'\phi_0'^* + \alpha_0\alpha_0^*\phi_0\phi_0^*)\,\mathrm{d}z \quad \text{and} \quad \mathscr{k} = \int_0^\infty \phi_0'\phi_0'^*\,\mathrm{d}z,$$

$$\alpha^{|u|} = \frac{1}{|u|}\frac{\partial|u|}{\partial x} = -\mathrm{Im}\,(\alpha_0 + \epsilon\alpha_1) + \epsilon\,\mathrm{Re}\left\{\frac{1}{\phi_0'}\partial_{x_1}\phi_0'\right\}, \tag{2.46}$$

$$\alpha^{|w|} = \frac{1}{|w|}\frac{\partial|w|}{\partial x} = -\mathrm{Im}\,(\alpha_0 + \epsilon\alpha_1) + \epsilon\,\mathrm{Re}\left\{\frac{1}{\alpha_0}\partial_{x_1}\alpha_0 + \frac{1}{\phi_0}\partial_{x_1}\phi_0\right\}. \tag{2.47}$$

The growth rate factors α^E, α^I and $\alpha^{|u|}$ were introduced by Gaster (1974), whilst $\alpha^{|w|}$ was used by Bridges & Morris (1987). The growth rate factors $\alpha^{|u|}$ and $\alpha^{|w|}$ have a dependence on z through their last term. Appropriate values of z are frequently chosen based on distinguished features of the eigenfunction. Thus Gaster evaluated $\alpha^{|u|}$ at values of z corresponding to the local maxima of $|u|$. There are normally two such maxima: one near the wall and one near the outer edge of the boundary layer, termed the inner and outer maximum respectively. Bridges & Morris defined a neutral curve criterion based on the evaluation of $\alpha^{|w|}$ at a point near $z = 2$.

2.5. *Extension to multi-layer walls*

The formulation for single-layer compliant walls developed in the preceding sections may be extended to multi-layer cases by replacing all the occurrences of the two-argument propagating matrix $\boldsymbol{P}(z_b, z_a)$ with the more general multi-layer propagation matrix defined below. Figure 1 shows an n-layer compliant wall which has its jth layer ($1 \leqslant j \leqslant n$) located between $z = z_{j-1}$ (top surface) and $z = z_j$ (bottom surface). For z_a in the rth layer and z_b in the sth layer ($1 \leqslant r \leqslant s \leqslant n$), the propagation matrix (which relates the displacement-stress vector at the two points, Yeo 1988) is given by

$$\boldsymbol{P}(z_b, z_a) = \boldsymbol{P}^{(s)}(z_b, z_{s-1})\,\boldsymbol{P}^{(s-1)}(z_{s-1}, z_{s-2}) \ldots \boldsymbol{P}^{(r+1)}(z_{r+1}, z_r)\,\boldsymbol{P}^{(r)}(z_r, z_a). \tag{2.48}$$

$\boldsymbol{P}^{(j)}(\xi, \vartheta) = \exp[(\xi - \vartheta)\,\boldsymbol{C}_0^{(j)}]$ is the propagation matrix of the jth layer, where $\boldsymbol{C}_0^{(j)}$ is the $\boldsymbol{C}_0$ matrix in the Appendix evaluated based on the material properties of the jth layer. Perfect bonding between adjacent layers has been assumed in deriving (2.48). In forming the boundary-condition matrices for the $O(\epsilon^0)$ and $O(\epsilon^1)$ problems, the z_1 for the single-layer case (see (2.34)) should be replaced with z_n, which is the bonded interface of the last (nth) layer with the rigid base.

2.6. *Aspects of numerical computation*

The $O(\epsilon^0)$ locally parallel flow eigenvalue problem (2.36) is solved by a spectral collocation procedure in which the eigenfunction ϕ_0 is expanded in terms of Chebyshev polynomials in z. The components of the basic flow are similarly represented. The homogeneous adjoint problem to (2.36) is solved using the same spectral collocation procedure, except that no iteration is required to find the adjoint eigenfunction φ because the eigenvalues of the adjoint problem are identical to those of (2.36). $\phi_0(x_1, z)$ is normalized such that $\phi_0'' = 1.0$ at $z = z_0$ for the case of rigid wall. For compliant walls, the same normalization is also adopted. All derivatives of $\phi_0(x_1, z)$ with respect to x_1 are performed using second-order-accurate central difference scheme, with regular verification of accuracy. The functions $C_{0\alpha}(x_1)$ and $C_{0\chi}(x_1)$ (see (2.11)) are determined from the solution of $\phi_0(x_1, z)$ at z_∞ and their derivatives with respect to x_1 are also computed using second-order central differencing. All integrals with respect to z are calculated using the fourth-order-accurate Simpson's rule.

3. Results and discussions

3.1. *Rigid-wall case*

Before proceeding to consider the more complex case of compliant walls, we first compare our non-parallel flow calculations against some of the rigid-wall results available in the literature. The non-parallel neutral stability curves based on the streamwise growth of the kinetic-energy integral E, the inner maximum of $|u|$ and $|w|$ at $z = 2.0$ were compared to the corresponding results of Gaster (1974), Bridges &

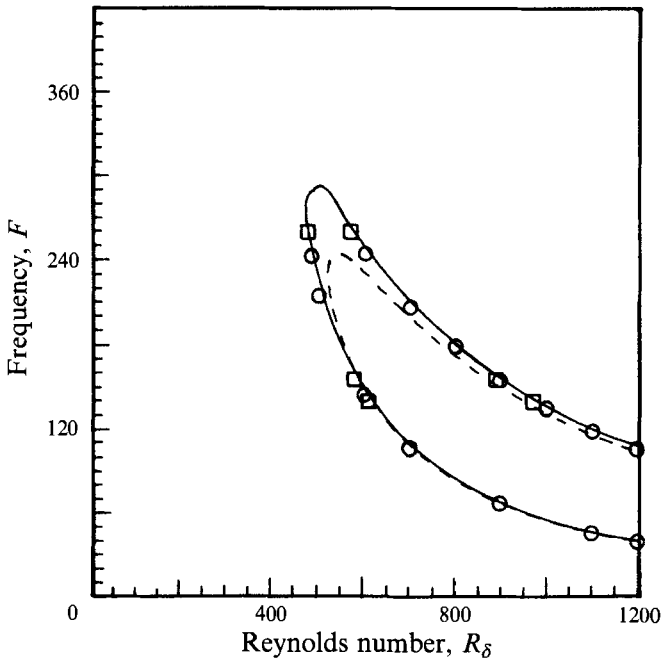

FIGURE 3. Neutral stability results for a rigid wall based on $\alpha^{(E)} = 0$: ——, present non-parallel results; ○, Gaster (1974); □, Fasel & Konzelmann (1990); ----, $-\mathrm{Im}\,(\alpha_0) = 0$ (parallel flow).

Morris (1987) and Fasel & Konzelmann (1990), all pertaining to the Blasius boundary layer. The agreement was very good in all cases. The results for the kinetic-energy integral E in particular is shown in figure 3, where the frequency of the perturbation is plotted along the ordinate as the parameter $F = [\omega^{(d)}\nu^{(d)}(U_\infty^{(d)})^{-2}] \times 10^6$. The very good agreement with the data points of Fasel & Konzelmann is especially significant because the latter's results were obtained from the direct integration of the Navier–Stokes equations, a distinctly different treatment from the eigenvalue-correction approach used by Gaster and the present work.

3.2. *Compliant walls*

Having thus established the consistency of our non-parallel flow calculations with available results in the literature on rigid walls, we now consider the case of compliant walls. The dynamical response of a compliant layer to a perturbation is dependent upon its material properties: the material density ρ, the elastic shear-wave speed C_t, the material damping coefficient d and the bulk modulus K (see §2.2). It is also dependent upon the thickness h of the layer. These are non-dimensionalized with respect to the free-stream speed $U_\infty^{(d)}$, the fluid density $\rho_f^{(d)}$ and a reference wall lengthscale $L_w^{(d)}$. The reference lengthscale $L_w^{(d)}$ is specified implicitly via the wall reference Reynolds number R_w (defined after (2.28)), which is assigned a value of 2×10^4 throughout. The compliant walls considered below have material density $\rho = 1.0$, which corresponds roughly to the use of rubber-type materials in water.

The non-parallel growth factors α^E and $\alpha^{|u|}$ are used in this paper to evaluate the importance and the effects of boundary-layer non-parallelism over compliant walls. These choices are to some extent arbitrary. Proper choices should be guided by the availability of specific data for comparison. However, detailed experimental data are not yet available. Also, our results are not directly (quantitatively) comparable to the

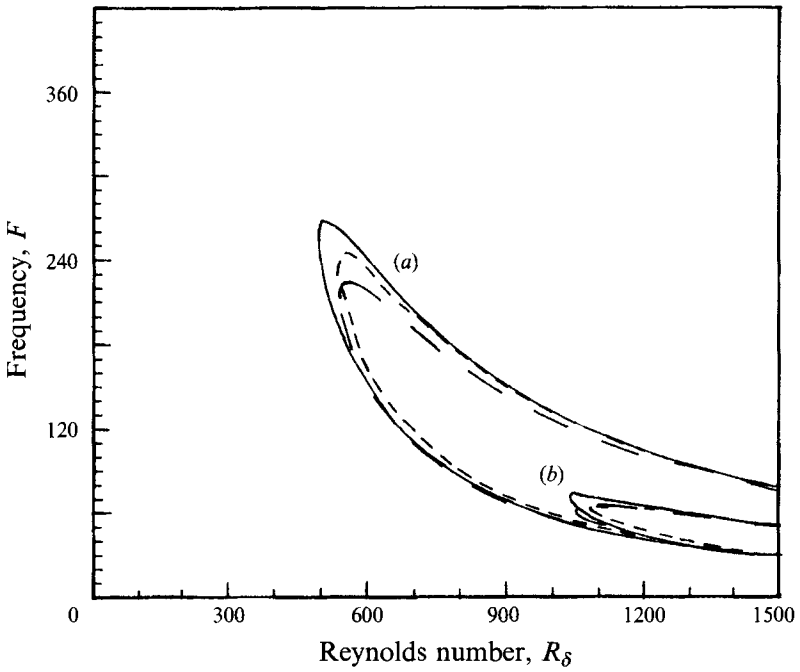

FIGURE 4. Neutral stability curves for single-layer walls with damping coefficient $d = 0.0049$, bulk modulus $K = 500$ and of different shear wave seed C_t and thickness h. (*a*) $C_t = 2.0$, $h = 1.0$; (*b*) $C_t = 0.7$, $h = 5.0$. ——, $\alpha^{(E)} = 0$; ----, $\alpha^{|u|} = 0$; ———, $-\mathrm{Im}\,(\alpha_0) = 0$ (parallel flow).

theoretical results of Carpenter & Sen (1990) owing to differences in the wall model. The growth factor α^E is chosen because the kinetic-energy integral E provides intuitively the best measure of the size of a disturbance at a streamwise station. However, E is a fairly cumbersome quantity to measure in practice. Because of the more widespread use of $|u|$ in experiments, it was decided also to include the growth factor $\alpha^{|u|}$, with $|u|$ being evaluated at the well-defined inner maximum.

We first examine the effects of boundary-layer non-parallelism on the compliant-wall TSI. Figure 4 shows the TSI regimes for two single-layer compliant walls based on the three measures of spatial growth: $-\mathrm{Im}\,(\alpha_0)$, α^E and $\alpha^{|u|}$. The softer wall, with a material $C_t = 0.7$ and $h = 5.0$, has a real shear modulus $\mathrm{Re}\,(G) = \rho C_t^2$ which is about one-eighth times that of the stiffer wall. We shall look at the two non-parallel criteria in turn. For the energy growth criterion, non-parallelism may be seen to be destabilizing along the upper branch and near the nose of the TSI regime for both of the walls. A reduction of critical Reynolds number Re_δ^{cr} is indicated for both walls. These trends are similar to those observable in figure 3 for the rigid wall. For the $|u|$ criterion, flow non-parallelism is also destabilizing along the upper branch of the TSI regimes. However, no significant change of Re_δ^{cr} is observed for the stiffer wall (which is in agreement with rigid-wall results not shown here), but a small increase in Re_δ^{cr} is seen for the much softer wall. The $|u|$ criterion also indicates a mild degree of stabilization along the lower branch of the regime. Overall, we note that the effects of flow non-parallelism on compliant-wall TSI are fairly mild.

To consider the effects of flow non-parallelism on the travelling-wave flutter (TWF) mode of instability, we need to move on to even softer walls. TWF starts to become important once the material shear wave speed C_t falls below the free-stream speed. Material damping can play an important role in suppressing and controlling the

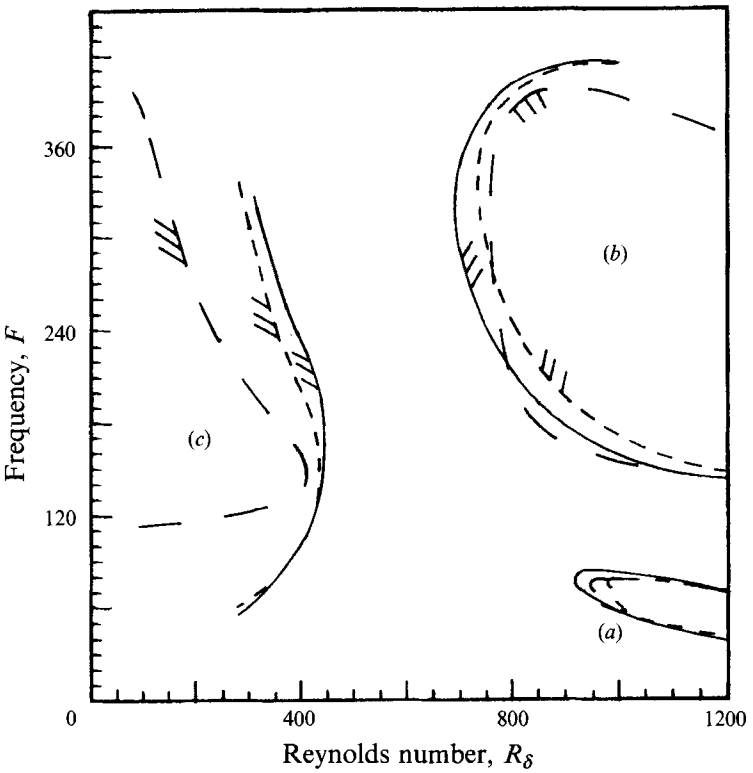

FIGURE 5. Neutral stability curves for a single-layer wall with $h = 1.0$, $K = 500$, $C_t = 0.7$ and $d = 0.0049$. (*a*) TSI, (*b*) B_1 TWF, (*c*) B_2 TWF. ——, $\alpha^{(E)} = 0$; - - - - -, $\alpha^{|u|} = 0$; ———, $-\mathrm{Im}\,(\alpha_0) = 0$ (parallel flow).

severity of the TWF. Figure 5 shows the TWF and TSI regimes for a single-layer compliant wall with $C_t = 0.7$ and layer thickness $h = 1.0$. The material damping has been kept at a low level to prevent the suppression of the TWF. The TWF instabilities exist in two disconnected parts, which are labelled B_1 and B_2 as in Yeo (1988). The unstable side of the neutral curves is marked by partial hatching. The B_1 regime is generically the same as the TWF regime on plate surfaces studied by Carpenter & Garrad (1985). The B_2 regime, which emerges at low R_δ, however, appears to have no equivalent on plate surfaces.

It can be seen in figure 5 that the effects of non-parallelism on TSI remain mild as before. Flow no-parallelism appears to have overall a destabilizing effect on the B_1 TWF according to the energy criterion. This destabilizing effect has been found to be generally mild, although somewhat stronger than for TSI at corresponding R_δ. In fact, non-parallelism may be seen to be slightly stabilizing along a short portion of the lower branch of the B_1 neutral curve. The effect of non-parallelism on the B_1 regime is, however, less regular for the $|u|$ criterion. Destabilization occurs along the upper branch, but significant stabilization may be seen along the lower branch. An analysis of the flow eigenfunctions along the B_1 neutral curve reveals that the fairly rapid z-shift of the inner maximum of $|u|$ is a significant factor contributing to the sensitivity of the $|u|$ criterion. The strongest effect of flow non-parallelism is, however, reserved for the low-R_δ B_2 TWF regime. The effect is one of destabilization, and it produces a significant enlargement of the instability domain. It is pertinent to note that the two non-parallel criteria, energy and $|u|$, are in reasonably good agreement in their

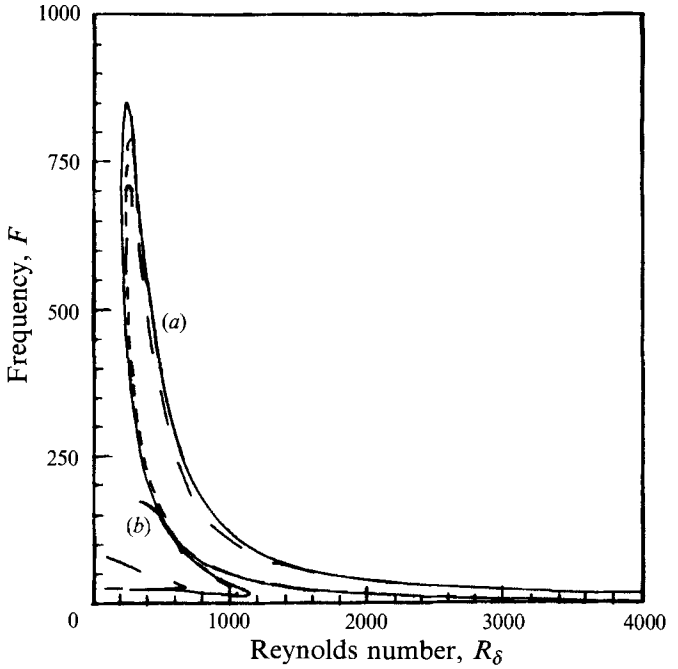

FIGURE 6. Neutral stability curves for a thick-layer wall with $h = 5.0$, $K = 500$, $C_t = 0.7$ and $d = 0.0294$. (*a*) TSI, (*b*) B_2 TWF. ——, $\alpha^{(E)} = 0$; -----, $\alpha^{|u|} = 0$; ———, $-\mathrm{Im}\,(\alpha_0) = 0$ (parallel flow).

prediction of the unstable domain, quite contrary to the preceding case for B_1 regime. The strong effect of flow non-parallelism on the B_2 modes is consistent with its low-R_δ origin.

Next we examine a compliant layer, figure 6, which is five times as thick as the preceding wall of figure 5, and possesses a much higher coefficient of material damping, $d = 0.0294$. The wall has been found to have significant potential for delaying transition according to the locally parallel flow calculations of Yeo (1988). The high level of damping effectively suppressed the B_1 TWF regime to a high Reynolds number R_δ beyond 4000 (and thus not reflected in the figure). The B_2 regime, owing to its low frequency, is not strongly inhibited by the high damping and remains clearly visible in figure 6. The amplification rates of the B_2 regime are, however, very low according to parallel-flow calculations and do not produce significant disturbance growth. A two-dimensional e^n ($n = 8.3$) calculation carried out by Yeo (1988) on the dominant TSI regime yielded a laminar–turbulent transition Reynolds number R_δ in excess of 5000, compared to 2900 for a rigid wall. The parallel and non-parallel flow neutral stability curves for the thick-layer wall are compared in figure 6. In spite of the greatly extended frequency range of the unstable TSI modes, which goes up as high as $F = 750$, the influence of flow non-parallelism appears to be rather small and similar to those of the preceding cases. The diminishing influence of non-parallelism with increasing R_δ is also clearly evident in the figure, which shows the TSI regime to a fairly large R_δ of 4000. As R_δ becomes large, the non-parallel neutral curves $\alpha^E = 0$ and $\alpha^{|u|} = 0$ converge to the parallel-flow neutral curve. Since the destabilization of TSI is fairly mild throughout the entire range of R_δ, laminar–turbulent transition via TSI modes is not expected to be significantly affected by boundary-layer non-parallelism. The rapidly diminishing importance of non-parallelism at high R_δ is also applicable to the B_1 TWF regime which is present beyond R_δ of 4000 (not shown). A very strong destabilizing

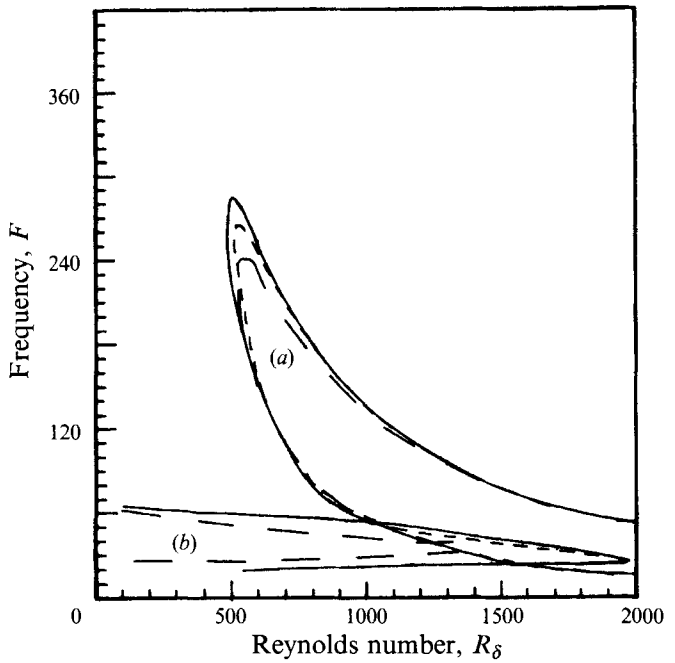

FIGURE 7. Neutral stability curves for a two-layer wall. Layer 1: $h = 0.1$, $C_t = 33.01$, $d = 0$, $K = 2360.7$. Layer 2: $h = 4.5$, $C_t = 0.7$, $d = 0.0049$, $K = 500$. (*a*) TSI, (*b*) B_2 TWF. ——, $\alpha^{(E)} = 0$; ----, $\alpha^{|u|} = 0$; ———, $-\mathrm{Im}\,(\alpha_0) = 0$ (parallel flow).

influence is, however, again observed for the low-R_δ B_2 TWF regime. The two non-parallel flow neutral criteria $\alpha^E = 0$ and $\alpha^{|u|} = 0$ are in approximate agreement as to the extent of the B_2 instability regime. The destabilization occurs primarily along the upper neutral branch and pushes the unstable B_2 regime to beyond the R_δ of 1100 from the value of 700 according to parallel-flow calculations. The non-parallel and parallel neutral curves are nearly coincident along the lower branch. The very considerable enlargement of the unstable B_2 TWF is in fact associated with a large increase in the disturbance growth rates due to non-parallel flow effects. Some details of B_2 growth rates will be given for the compliant wall examined in the next section.

3.3. *A two-layer compliant wall*

The next wall to be examined is a two-layer compliant wall comprising a thin layer of a stiff material (large elastic shear modulus) bonded onto a much thicker layer of a soft material. Such a two-layer wall configuration was employed by Gaster (1987) (see also Willis 1986) in his experiment, and found to possess the ability to reduce the growth rates of TSI waves when tailored with suitable properties. Neutral stability curves for the wall based on parallel-flow calculations and the two non-parallel flow criteria are illustrated in figure 7. It is noted that the effects of flow non-parallelism on the TSI regime are again fairly mild and similar to that for single-layer compliant walls. The B_1 regime has in this case been suppressed to a high Reynolds number by the relatively high stiffness of the top layer. The B_2 TWF regime is again strongly destabilized by non-parallel effects, as in the preceding cases. Besides a significant broadening of the frequency band of the regime, non-parallel effects cause the unstable B_2 regime to extend to R_δ of nearly 2000; both non-parallel criteria are in good general agreement.

The enlargement of the B_2 regime has already been mentioned to be associated with the large disturbance growth rates produced by non-parallel effects. Figure 8(*a*) shows

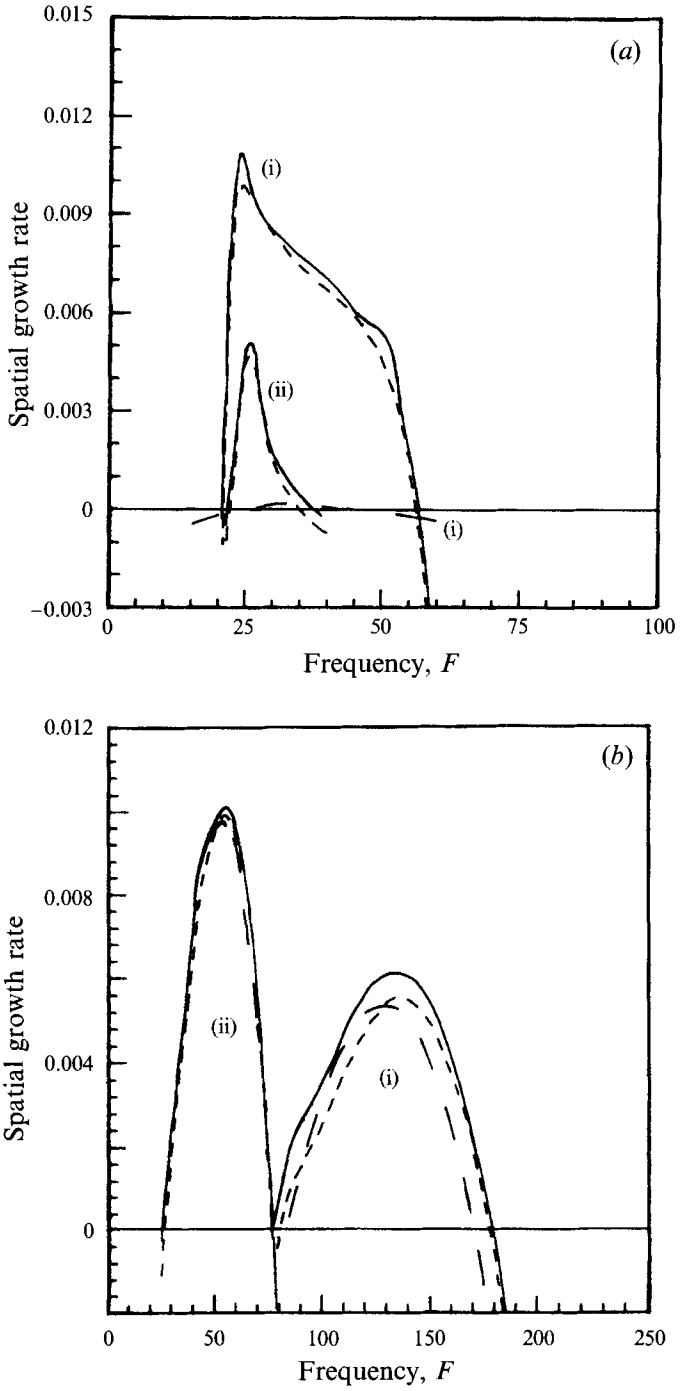

FIGURE 8. Spatial amplification rates of (*a*) B_2 TWF regime and (*b*) TSI regime for the compliant wall of figure 7. (i) $R_\delta = 800$, (ii) $R_\delta = 1500$. ——, $\frac{1}{2}\alpha^{(E)}$; - - - - -, $\alpha^{|u|}$; — — —, $-\mathrm{Im}\,(\alpha_0)$ (parallel flow).

the spatial growth rates $-\mathrm{Im}\,(\alpha_0)$, $\frac{1}{2}\alpha^E$ and $\alpha^{|u|}$ for the unstable B_2 modes at $R_\delta = 800$ and 1500 as a function of frequency F. At $R_\delta = 1500$, there are no unstable B_2 modes according to parallel-flow theory. At $R_\delta = 800$, it can be seen that the non-parallel growth rates are so much higher than the growth rates predicted by parallel-flow

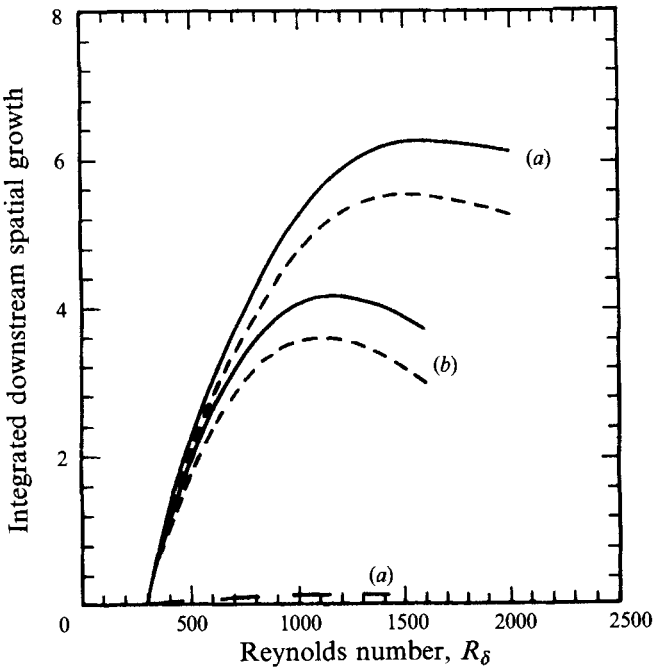

FIGURE 9. Integrated streamwise amplification of fixed-frequency waves by the B_2 TWF regime in figure 7: (*a*) $F = 35$, (*b*) $F = 50$. ——, $\ln(E^{1/2}/E_0^{1/2})$; - - - - -, $\ln(|u|/|u_0|)$; — — —, $\ln(|A|/|A_0|)$ (parallel flow).

theory. The growth rates based on the two non-parallel criteria are in approximate agreement both in terms of magnitude and frequency range. The corresponding growth rates for the TSI regimes at the same set of Reynolds numbers are given in figure 8(*b*). These curves confirm what we have qualitatively noted above that non-parallel effects are only mildly destabilizing to the TSI. Comparing the growth rates of the two instabilities given in figures 8(*a*) and 8(*b*), it is observed that the non-parallel B_2 TWF modes at $R_\delta = 800$ actually develop higher maximum growth rates than corresponding TSI regimes. This is in sharp contrast with the parallel-flow calculations which show a TSI regime dominating a B_2 TWF regime of very small growth rates. This result highlights the overwhelming importance of non-parallel flow effects for the B_2 regimes. For highly compliant walls especially, the adverse influence of non-parallelism may reach out to fairly large R_δ (such as in figure 7), where its effects on TSI has appeared to be negligible. Thus the nature of the instability can make an important difference to the effects of boundary-layer non-parallelism.

To further evaluate the importance of boundary-layer non-parallelism and assess the possible role that an enhanced B_2 TWF regime may play in triggering early transition of the flow to a turbulent state, the integrated streamwise growths of fixed-frequency unstable B_2 modes are also examined. Figure 9 shows the cumulative streamwise amplification of the B_2 modes for the two-layer wall at the frequencies of $F = 35$ and 50. Integration was commenced at $R_\delta = 300$. From figure 9, we can see that the streamwise cumulative growth of some unstable B_2 modes far exceeds the prediction of parallel-flow theory with amplitude ratio reaching beyond e^6, where e^n with $8 < n < 11$ have frequently been used to correlate with the onset of transition. This suggests that the B_2 TWF may be a cause for early transition. This is particularly important in situations where the level of turbulence in the oncoming stream is significant or the

magnitude of disturbances in the leading-edge region of the boundary layer is high. The possible presence of strong B_2 modes also suggests that inviscid hydroelastic-type theory (see Carpenter & Garrad 1988) may overestimate the true onset (critical) flow speed for strong TWF instability. The hydroelastic theory approximates the behaviour of B_1 TWF at large R_δ reasonably well. Since the destabilizing influence of non-parallelism on the TSI of the two-layer wall is generally small, and moreover diminishes to negligible levels at higher R_δ, the cumulative streamwise growth of the TSI modes on the wall will only be slightly affected by non-parallel effects. This implies that for all practical purposes the transition of the flow, if it occurs via TSI modes, will be but little affected by non-parallel effects.

The above two-layer compliant wall with its top layer of stiff material bears a significant degree of similarity with the bending plate on elastic foundation model studied by Carpenter and coworkers. Carpenter & Sen (1990) noted that the TSI regime over their wall, which was an approximate model of Kramer's (1960) best coating (but without the damping fluid), was only mildly destabilized by non-parallelism. This result is in qualitative agreement with ours for both single- and two-layer walls. No comparison of results can be made for the TWF modes, however, since Carpenter & Sen did not consider them.

3.4. *Suppression of unstable B_2 modes and three-dimensional aspects*

The susceptibility of compliant surfaces to low-R_δ B_2 TWF (a FISI) instability does not imply that they are therefore incapable of delaying laminar–turbulent transition. Compliant surfaces come in useful to stabilize the TSI mainly in the range of Reynolds number R_δ from 10^3 to say 10^4. The concern with low-R_δ B_2 instability is actually one of preventing it from triggering premature transition. This can be achieved by employing a panel of stiffer material up front from the leading-edge region up to an appropriate R_δ, say 700. This will eliminate the most dominant portion of the B_2 TWF instability. This multi-panel approach, which involves using compliant panels of different properties, was in fact employed by Carpenter (1991) for optimizing the transition-delaying performance of plate-type surfaces. Alternatively, the low-R_δ B_2 instability may be resisted by thinning the compliant layer progressively towards the leading edge. Reduction in layer thickness increases wall stiffness which resists the B_2 instability. For streamlined bodies, the B_2 instability may also possibly be inhibited by a suitably profiled nose which produces a favourable pressure gradient and highly stable flow. Properly applied, these measures to control the low-R_δ unstable B_2 modes should not unduly affect the stabilizing quality of a compliant wall with respect to the TSI where it matters most.

The detailed analysis of non-parallel flow effects on three-dimensional obliquely propagating wave modes is rather involved. However, some intuitive conjectures as to their possible influence may be made on the basis of the Stuart-type transformation used by Yeo (1986, 1992) in his locally parallel flow study. Under the transformation, an oblique wave propagating at an angle θ to the downstream direction perceives a boundary layer with the velocity field ($U\cos\theta$, W). The horizontal component $U\cos\theta$ diminishes in magnitude relative to the vertical component W as θ is increased from zero. The perceived boundary layer therefore exhibits a growing degree of flow divergence with increasing θ. The increase in flow divergence marks an enhancement of non-parallel effects on the three-dimensional waves relative to those on two-dimensional modes at the same Reynolds number R_δ. For three-dimensional oblique FISI wave modes, the increased destabilizing influence of non-parallelism is opposed by an apparent increase in the wall stiffness moduli (rescaling by $(\cos\theta)^{-2}$) due to

reduction in perceived free-stream speed. The latter is known to have a strong stabilizing effect on the FISI (see Yeo 1986, 1992). Taken together, it is expected that the non-parallel stability of the flow to three-dimensional FISI modes, which include the low-R_δ B_2 TWF, will not be significantly worse than its non-parallel stability to two-dimensional FISI modes.

The situation for TSI appears to be somewhat less desirable. This is because the increase in apparent wall stiffness adds to rather than subtracts from the destabilizing influence of increased non-parallelism experienced by the three-dimensional TSI modes. At large angle of propagation θ, the compliant wall subjected to stiffness rescaling approaches the rigid-wall behaviour. The perceived mean flow field subjected to a corresponding velocity rescaling acquires the Blasius mean flow $(U, W(\cos\theta)^{-1})$ at the reduced Reynolds number of $R_\delta \cos\theta$. This implies that at large θ, the three-dimensional compliant-wall TSI mode is subjected to non-parallel effects similar to those for rigid-wall two-dimensional TSI at low Reynolds number. This large-θ rigid-wall behaviour of compliant wall three-dimensional TSI appears to persist even to large Reynolds numbers because the reduction in the non-parallel effect due to increase in R_δ (for example $W = O(R_\delta^{-1})$) is ultimately opposed by increased flow divergence at sufficiently large θ, up to a limiting $\theta < 90°$ beyond which no TSI exist. A limiting θ exists because there is no rigid-wall TSI when the Reynolds number $R_\delta \cos\theta$ of the equivalent two-dimensional case is sufficiently low. The presence of the rigid-wall-related destabilizing non-parallel influence at large θ and large R_δ is not expected to have unduly serious consequences for overall stability and transition however. This is because firstly the destabilizing non-parallel influence for a rigid wall is rather mild and secondly the more dominant compliant-wall TSI modes at large R_δ usually occur for fairly small θ, at which non-parallel effects should be quite negligible.

3.5. *Further remarks*

Because of the perturbative nature of the present work, some comments on the accuracy of the results are in order. The studies that have been done on boundary-layer non-parallelism to date have attempted only to correct for the leading-order non-parallel effects, $O(\epsilon^1)$. Intuitively, this leading-order correction appears to be quite adequate because ϵ is generally very small in the range of Reynolds numbers that is of interest; $\epsilon < 0.0043$ for $R_\delta > 400$. Issues and problems connected with the implementation of higher-order corrections have in fact been discussed by Gaster (1974). What seems clear is that extension to the next and higher orders is a highly non-trivial problem. The recent non-parallel study by Fasel & Konzelmann (1990) based on direct Navier–Stokes simulation sheds some important light here. In achieving very good agreement with the established $O(\epsilon^1)$ calculations of Gaster (1974), Bridges & Morris (1987) and others, they have shown that the $O(\epsilon^1)$ corrections are in fact completely adequate in capturing the effects of boundary-layer divergence, at least in the R_δ range covered by their calculations, which is down to R_δ of around 450. This adequacy of the $O(\epsilon^1)$ correction is likely to extend to the compliant wall case because the 'degree' of non-parallelism is determined solely by the flow, which is common to both cases. The uniformly thick compliant layers have no innate non-parallelism, but merely respond to and reflect the non-parallelism of the flow. We can therefore expect the non-parallel effects at the same Reynolds number to be represented to the same accuracy, with possibly some influence from frequency and wavenumber. As one gets to even lower R_δ, the need to take into account higher-order non-parallel effects undoubtedly increases. However, if the very good agreement between the $O(\epsilon^1)$-corrected results and direct Navier–Stokes simulations is anything to go by, we can expect the effects of the

next order of correction to be quite small for R_δ down to about say 350 (the value is only an intuitive guess). The results we have obtained for the B_2 TWF are therefore quite reliable. It may be recalled that in some cases the B_2 regime actually stretched to fairly large R_δ (nearly 2000 for the two-layer wall) where the accuracy of the $O(\epsilon^1)$ correction is not in doubt. Hence the results for the B_2 regime are with great certainty qualitatively correct. Quantitatively, it is believed that the B_2 results are quite good to R_δ as low as 350.

As one progresses to even lower R_δ, non-parallel effects will increase more dramatically. In the range of very low R_δ, the study of boundary-layer stability based upon the treatment of non-parallelism as a higher-order effect, tacked onto a locally parallel theory, may not be the most ideal approach. An alternative is suggested by the recent work of Goldstein (1983) on boundary-layer receptivity. The unsteady motion in the region of the flat plate stretching from the vicinity of the leading edge to distances $x^{(d)} = O(U_\infty^{(d)}/\omega^{(d)})$ (or $R_\delta = O(1720 \times F^{-1/2})$) is governed by the linearized unsteady boundary-layer equation (UBL). The UBL equation incorporates the influence of boundary divergence on the unsteady motion to its lowest order. Goldstein showed that the solutions of the UBL equation (in the region where divergence is strong) are smoothly connected to the solutions of the non-parallel OS equation, which applies further downstream. This suggests that the UBL equation in a suitable homogeneous form may be useful for the study of instability at very low R_δ. By incorporating divergence to the lowest order, the UBL equation may be expected to capture the non-parallel effects more efficiently than an approach based on developing successive corrections. In fact, the UBL equation and the non-parallel OS equation are derivatives of a common and more complex equation (2.19) of Goldstein (1983) in the appropriate streamwise limits. Much work may be needed to adapt the UBL equation for stability study, however. The usual normal-mode analysis does not work because the UBL equation has explicit dependence on the stream coordinate. A receptivity study based on the UBL equation will also, on the other hand, be extremely useful in clarifying how the various compliant-wall instabilities, and in particular the B_2 TWF which exists in this sensitive region, may be excited by external perturbations.

4. Conclusions

The two-dimensional non-parallel linear stability of zero-pressure-gradient boundary layers over compliant walls was studied. Corrections to the spatial amplification rate of standard locally parallel-flow theory based on various growth criteria were obtained for leading-order non-parallel effects. The results indicate that the influence of boundary-layer non-parallelism is in general one of destabilization.

For the Tollmien–Schlichting instability (TSI), the destabilizing influence of non-parallelism has been found to be fairly mild. The destabilization of B_1 travelling-wave flutter (TWF) is also generally mild, although a little stronger than for the TSI. The destabilizing effect on the low-Reynolds-number B_2 TWF regime has, however, been found to be strong, so that a locally parallel theory may grossly underestimate the spatial growth of the instability. In general the destabilizing effect of non-parallelism was found to diminish with increasing Reynolds number.

The financial support of the National University of Singapore for Mr W. K. Chong under Grant No. 910670 is gratefully acknowledged.

Appendix

Some functions and matrices in equations (2.9), (2.22), (2.25), (2.32) and (2.33) are listed below.

$$F_1 = (B_1 + B_2\,\partial_z^2)(\partial_{x_1}\phi_0) + (\partial_{x_1}\alpha_0)(B_3 + B_4\,\partial_z^2)\,\phi_0 + (B_5 + B_6\,\partial_z + B_7\,\partial_z^2 + B_8\,\partial_z^3)\,\phi_0,$$
$$F_2 = (B_1 + B_2\,\partial_z^2)\,\phi_0,$$

where

$$B_1 = 3\mathrm{i}\alpha_0 U_0 + \mathrm{i}\alpha_0^{-1}(\partial_z^2 U_0) - 2\mathrm{i}\omega + 4\alpha_0^2 R_\delta^{-1}, \quad B_2 = -\mathrm{i}\alpha_0^{-1} U_0 - 4R_\delta^{-1},$$
$$B_3 = 3\mathrm{i}U_0 + \mathrm{i}\alpha_0^{-1}\omega + 6\alpha_0 R_\delta^{-1}, \quad B_4 = -2\alpha_0^{-1} R_\delta^{-1},$$
$$B_5 = 0, \quad B_6 = \mathrm{i}\alpha_0^{-1}(\alpha_0^2 + \partial_z^2)\,W_1,$$
$$B_7 = 0, \quad B_8 = -\mathrm{i}\alpha_0^{-1} W_1.$$

$$\boldsymbol{C}_0 = \begin{bmatrix} 0 & -\mathrm{i}\alpha_0 & G^{-1} & 0 \\ -\mathrm{i}\alpha_0\lambda(\lambda+2G)^{-1} & 0 & 0 & (\lambda+2G)^{-1} \\ -\rho\omega^2 + 4G\alpha_0^2(\lambda+G)(\lambda+2G)^{-1} & 0 & 0 & -\mathrm{i}\alpha_0\lambda(\lambda+2G)^{-1} \\ 0 & -\rho\omega^2 & -\mathrm{i}\alpha_0 & 0 \end{bmatrix},$$

$$\boldsymbol{C}_2 = \begin{bmatrix} 0 & -1 & 0 & 0 \\ C_{2a} & 0 & 0 & 0 \\ C_{2b} & C_{2c} & 0 & 0 \\ 0 & 0 & -1 & 0 \end{bmatrix}, \quad \boldsymbol{C}_1 = \begin{bmatrix} 0 & 0 & 0 & 0 \\ 0 & 0 & 0 & 0 \\ C_{1a} & 0 & 0 & 0 \\ 0 & 0 & 0 & 0 \end{bmatrix},$$

$$C_{2a} = -\lambda/(\lambda+2G), \quad C_{2b} = -\mathrm{i}\alpha_0(\lambda^2 + 8\lambda G + 8G^2)/(\lambda+2G), \quad C_{2c} = -\lambda\,\partial_z,$$
$$C_{1a} = -\mathrm{i}(\lambda+2G)\,\partial_{x_1}\alpha_0.$$

$$\boldsymbol{F}_1 = \begin{bmatrix} 0 & F_{1a} & 0 & 0 \\ F_{1b} & 0 & 0 & 0 \\ F_{1c} & 0 & 0 & F_{1b} \\ 0 & 0 & F_{1a} & 0 \end{bmatrix},$$

$$F_{1a} = -\mathrm{i}\,\partial_{x_1}\alpha_0, \quad F_{1b} = -\mathrm{i}\lambda(\lambda+2G)^{-1}\partial_{x_1}\alpha_0, \quad F_{1c} = 8G(\lambda+G)(\lambda+2G)^{-1}\alpha_0\,\partial_{x_1}\alpha_0.$$

$$\boldsymbol{Q}_c = \begin{bmatrix} \mathrm{i}U_0'\alpha_0\omega^{-2} & \mathrm{i}\omega^{-1} & 0 & 0 \\ \alpha_0\omega^{-1} & 0 & 0 & 0 \\ R_w^{-1}(\alpha_0^2 + U_0''\alpha_0\omega^{-1}) & 0 & R_w^{-1} & 0 \\ -U_0' & -(\omega/\alpha_0 + 3\mathrm{i}\alpha_0 R_w^{-1}) & 0 & -(\mathrm{i}\alpha_0 R_w)^{-1} \end{bmatrix}.$$

$$\boldsymbol{D}_1 = \begin{bmatrix} 0 & 0 & 0 & 0 \\ 0 & 0 & 0 & 0 \\ D_{1a} & D_{1b} & 0 & 0 \\ D_{1c} & D_{1d} & 0 & D_{1e} \end{bmatrix}, \quad \boldsymbol{D}_2 = \begin{bmatrix} D_{2a} & 0 & 0 & 0 \\ D_{2b} & 0 & 0 & 0 \\ D_{2c} & 0 & 0 & 0 \\ 0 & D_{2d} & 0 & D_{2e} \end{bmatrix},$$

$$D_{1a} = -\mathrm{i}R_w^{-1}(\partial_{x_1}\alpha_0 - U_0'\alpha_0\omega^{-2}\partial_{x_1}U_0'), \quad D_{1b} = \mathrm{i}(\omega R_w)^{-1}\partial_{x_1}U_0',$$
$$D_{1c} = (\alpha_0(\omega R_w)^{-1}W_1'' + (\mathrm{i}\alpha_0)^{-1}\partial_{x_1}U_0'), \quad D_{1d} = \mathrm{i}\omega\alpha_0^{-3}\partial_{x_1}\alpha_0, \quad D_{1e} = \alpha_0^{-3}R_w^{-1}\partial_{x_1}\alpha_0,$$
$$D_{2a} = U_0'\omega^{-2}, \quad D_{2b} = -\mathrm{i}\omega^{-1}, \quad D_{2c} = -2\mathrm{i}\alpha_0 R_w^{-1},$$
$$D_{2d} = -(\mathrm{i}\omega\alpha_0^{-2} + 3R_w^{-1}), \quad D_{2e} = -(\alpha_0^2 R_w)^{-1}.$$

$$\boldsymbol{E}_1 = \begin{bmatrix} E_{1a} & 0 & 0 & 0 \\ E_{1b} & 0 & 0 & 0 \\ E_{1c} & 0 & 0 & 0 \\ E_{1d} & E_{1e} & 0 & E_{1f} \end{bmatrix},$$

$$E_{1a} = \mathrm{i}\omega^{-2}(U_1'\partial_{x_1}\alpha_0 - \alpha_0 W_1''), \quad E_{1b} = \omega^{-1}\partial_{x_1}\alpha_0, \quad E_{1c} = 2\alpha_0 R_w^{-1}\partial_{x_1}\alpha_0,$$
$$E_{1d} = W_1'', \quad E_{1e} = (\omega\alpha_0^{-2} - 3\mathrm{i}R_w^{-1})\partial_{x_1}\alpha_0, \quad E_{1f} = (\mathrm{i}\alpha_0^2 R_w)^{-1}\partial_{x_1}\alpha_0.$$

REFERENCES

BARRY, M. D. J. & ROSS, M. A. S. 1970 The flat plate boundary layer. Part 2. The effect of increasing thickness on stability. *J. Fluid Mech.* **43**, 813.

BENJAMIN, T. B. 1960 Effects of a flexible boundary on hydrodynamic stability. *J. Fluid Mech.* **9**, 513.

BENJAMIN, T. B. 1963 The three-fold classification of unstable disturbances in flexible surfaces bounding inviscid flows. *J. Fluid Mech.* **16**, 436.

BLAND, D. R. 1960 *Linear Viscoelasticity*. Pergamon.

BOUTHIER, M. 1972 Stabilité linéaire des écoulements presque parallèles. *J. Méc.* **11**, 599.

BOUTHIER, M. 1973 Stabilité linéaire des écoulements presque parallèles. Partie *II*. La couche limite de Blasius. *J. Méc.* **12**, 75.

BRIDGES, T. J. & MORRIS, P. J. 1987 Boundary layer stability calculations. *Phys. Fluids* **30**, 3351.

CARPENTER, P. W. 1990 Status of transition delay using compliant walls. *Viscous Drag Reduction in Boundary layers: Progress in Astronautics & Aeronautics, AIAA* (ed. D. M. Bushnell & J. N. Hefner), **123**, 79.

CARPENTER, P. W. 1991 The optimization of multiple-panel compliant walls for delay of laminar-turbulent transition. *AIAA Paper* 91-1772.

CARPENTER, P. W. & GARRAD, A. D. 1985 The hydrodynamic stability of flow over Kramer-type compliant surfaces. Part 1. Tollmien–Schlichting instabilities. *J. Fluid Mech.* **155**, 465.

CARPENTER, P. W. & GARRAD, A. D. 1986 The hydrodynamic stability of flow over Kramer-type compliant surfaces. Part 2. Flow-induced surface instabilities. *J. Fluid Mech.* **170**, 199.

CARPENTER, P. W. & MORRIS, P. J. 1990 The effects of anisotropic wall compliance on boundary-layer stability and transition. *J. Fluid Mech.* **218**, 171.

CARPENTER, P. W. & SEN, P. K. 1990 Effects of boundary-layer growth on the linear regime of transition over compliant walls. In *Laminar–Turbulent Transition, IUTAM Symp. Toulouse/ France*, p. 123.

CODDINGTON, E. A. & LEVINSON, N. 1955 *Theory of Ordinary Differential Equations*. McGraw-Hill.

CRAIK, A. D. D. 1966 Wind-generated waves in thin liquid films. *J. Fluid Mech.* **26**, 369.

CRAIK, A. D. D. 1971 Nonlinear resonant instabilities in boundary layers. *J. Fluid Mech.* **50**, 393.

DRAZIN, P. G. & REID, W. H. 1981 *Hydrodynamic Stability*. Cambridge University Press.

FASEL, H. & KONZELMANN, U. 1990 Non-parallel stability of a flat-plate boundary layer using the complete Navier–Stokes equations. *J. Fluid Mech.* **221**, 311.

GASTER, M. 1974 On the effects of boundary-layer growth on flow stability. *J. Fluid Mech.* **66**, 465.

GASTER, M. 1987 Is the dolphin a red herring. In *Proc. IUTAM Symp. on Turbulence Management Relaminarization, Bangalore, India*, p. 285.

GILBERT, F. & BACKUS, G. E. 1966 Propagation matrices in elastic wave and vibration problems. *Geophysics* **31**, 326.

GOLDSTEIN, M. E. 1983 The evolution of Tollmien–Schlichting waves near a leading edge. *J. Fluid Mech.* **127**, 59.

GROSSKREUTZ, R. 1971 Wechselwirkungen zwischen turbulenten Grenzschichten und weichen Wanden. *Max-Planck Institut fur Stromungsforschung, Gottingen, Rep.* 53.

HERBERT, T. 1984 Analysis of subharmonic route to transition in boundary layers. *AIAA Paper* 84-0009.

JOSLIN, R. D. & MORRIS, P. J. 1992 Effect of compliant walls on secondary instabilities in boundary-layer transition. *AIAA J.* **30**, 332.

JOSLIN, R. D., MORRIS, P. J. & CARPENTER, P. W. 1991 The role of three-dimensional instabilities in compliant wall boundary-layer transition. *AIAA J.* **29**, 1603.

KRAMER, M. O. 1960 Boundary layer stabilization by distributed damping. *J. Am. Soc. Naval Engng* **73**, 25.

LANDAHL, M. T. 1962 On the stability of a laminar incompressible boundary layer over a flexible surface. *J. Fluid Mech.* **13**, 609.

RILEY, J. J., GAD-EL-HAK, M. & METCALFE, R. W. 1988 Compliant coatings. *Ann. Rev. Fluid Mech.* **20**, 393.

ROSS, J. A., BARNES, F. H., BURNS, J. G. & ROSS, M. A. S. 1970 The flat plate boundary layer. Part 3. Comparison of theory with experiment. *J. Fluid Mech.* **43**, 819.

SARIC, W. S. & NAYFEH, A. H. 1975 Nonparallel stability of boundary-layer flows. *Phys. Fluids* **18**, 945.

SARIC, W. S. & NAYFEH, A. H. 1977 Nonparallel stability of boundary layers with pressure gradients and suction. *AGARD Conf. Proc.* **224**, paper 6.

SCHUBAUER, G. B. & SKRAMSTAD, H. K. 1947 Laminar boundary-layer oscillations and transition on a flat plate. *J. Res. Natl Bur. Stand.* **38**, 251.

SHEN, S. F. 1954 Calculated amplified oscillations in the plane Poiseuille and Blasius flows. *J. Aero. Sci.* **21**, 62.

SMITH, F. T. 1979 On the non-parallel flow stability of the Blasius boundary layer. *Proc. R. Soc. Lond.* A **336**, 91.

THOMAS, M. D. 1992 On the resonant triad interaction in flows over rigid and flexible boundaries. *J. Fluid Mech.* **234**, 417.

VAN STIJN, TH. L. & VAN DE VOOREN, A. I. 1983 On the stability of almost parallel boundary layer flows. *Computers Fluids* **10**, 223.

WILLIS, G. J. K. 1986 Hydrodynamic stability of boundary layers over compliant surfaces. PhD thesis, University of Exeter.

YEO, K. S. 1986 The stability of flow over flexible surfaces. PhD thesis, University of Cambridge.

YEO, K. S. 1988 The stability of boundary-layer flow over single- and multi-layer viscoelastic walls. *J. Fluid Mech.* **196**, 359.

YEO, K. S. 1990 The hydrodynamic stability of boundary-layer over a class of anisotropic compliant walls. *J. Fluid Mech.* **220**, 125.

YEO, K. S. 1992 The three-dimensional stability of boundary-layer flow over compliant walls. *J. Fluid Mech.* **238**, 537.

YEO, K. S., KHOO, B. C. & CHONG, W. K. 1992 The linear stability of boundary-layer flow over compliant walls – effects of wall mean state. In *Proc. 2nd Intl Offshore & Polar Engng Conf., San Francisco, June 14–19*, vol. 3, p. 245.

YEO, K. S., KHOO, B. C. & CHONG, W. K. 1994 The linear stability of boundary-layer flow over compliant walls – the effects of the wall's mean state induced by flow loading. *J. Fluids Struct.* (to appear).